Geol. Mag. **152** (*4*), *2015, pp. 648–667. © Cambridge University Press 2014*
doi:10.1017/S0016756814000569

Building up of a nested granite intrusion: magnetic fabric, gravity modelling and fluid inclusion planes studies in Santa Eulália Plutonic Complex (Ossa Morena Zone, Portugal)

H. SANT'OVAIA*†, P. NOGUEIRA‡, J. CARRILHO LOPES§, C. GOMES¶, M.A. RIBEIRO*, H.C.B. MARTINS*, A. DÓRIA*, C. CRUZ*, L. LOPES‖, R. SARDINHA‖, A. ROCHA¶ & F. NORONHA*

*Geology Centre of Porto University, Department of Geosciences, Environment and Spatial Planning, Faculty of Sciences of Porto University, Rua do Campo Alegre, 4169-007 Porto, Portugal
‡Geology Centre of Porto University, Geosciences Department of Évora University, Largo dos Colegiais 2, 7004-516 Évora, Portugal
§Geology Centre of Lisbon University, Geosciences Department of Évora University, Largo dos Colegiais 2, 7004-516 Évora, Portugal
¶Geophysics Centre of University of Coimbra, Department of Earth Sciences, Faculty of Sciences and Technology of University of Coimbra, Largo Marquês de Pombal, 3000-272 Coimbra, Portugal
‖Geosciences Department of Évora University, Largo dos Colegiais 2, 7004-516 Évora, Portugal

(*Received* 27 December 2013; *accepted* 10 September 2014; *first published online* 14 November 2014)

Abstract – The Santa Eulália Plutonic Complex (SEPC), located in the Ossa Morena Zone (south Portugal), is composed of a medium- to coarse-grained pink granite (G0-type) and a central grey medium-grained biotite granite (G1-type). Available Rb–Sr data indicates an age of 290 Ma. An emplacement model for the SEPC is proposed, taking into account magnetic fabric, 2D gravity modelling and fluid inclusion planes studies. The G0 and G1 types demonstrate different magnetic behaviour: G0 is considered a magnetite-type granite and G1 is an ilmenite-type granite. The formation of G0 required oxidized conditions related to the interaction of mafic rocks with a felsic magma. The 2D gravity modelling and subvertical magnetic lineations show that the feeder zone of the SEPC is located in the eastern part of the pluton, confirming the role of the Assumar and Messejana Variscan faults in the process of ascent and emplacement. The magma emplacement was controlled by ENE–WSW planar anisotropies related to the final brittle stages of the Variscan Orogeny. The emplacement of the two granites was almost synchronous as shown by their gradational contacts in the field. The magnetic fabric however suggests emplacement of the G0-type first, closely followed by emplacement of the G1-type, pushing the G0 laterally which becomes more anisotropic towards the margin. The G1-type became flattened, acquiring a dome-like structure. The SEPC is a nested pluton with G0-type granite assuming a tabular flat shape and G1-type forming a rooted dome-like structure. After emplacement, SEPC recorded increments of the late Variscan stress field documented by fluid inclusion planes in quartz.

Keywords: anisotropy of magnetic susceptibility, isothermal remanent magnetization, fluid inclusion planes, 2D gravity modelling, magma emplacement, Variscan Orogeny.

1. Introduction

The Ossa Morena Zone is one of the zones of the Iberian massif which is considered to have become accreted to the Iberian autochthonous terrane during the Cadomian Orogeny (e.g. Quesada, 2006; Ribeiro *et al.* 2007, 2010). However, the time of accretion of the Ossa Morena Zone is not consensual among the scientific community. Some authors consider that the accretion is of Variscan age (e.g. Matte, 2001; Simancas *et al.* 2001, 2003). To the north, the Ossa Morena Zone is limited by the Coimbra–Cordoba Shear Zone (CCSZ) which is considered a Cadomian suture, reactivated as a Variscan flower structure. To the south, the suture between the Ossa Morena Zone and the South Portuguese Terrane corresponds to the SW Iberia Variscan suture (Munhá *et al.* 1986; Quesada *et al.* 1994; Fonseca, 1995; Fonseca *et al.* 1999; Ribeiro *et al.* 2007, 2010).

The Ossa Morena Zone is characterized by a polyphase ductile deformation and metamorphism resulting in regional shear zones, with a NW–SE orientation materialized by schistosity (Araújo *et al.* 2013) and affected by weak crenulation. The intensity of the deformation increases in the direction of the major shear zone, the Coimbra–Cordoba Shear Zone (Fig. 1). The last ductile deformation phase is dated at 306 Ma (Moita *et al.* 2005; Ribeiro *et al.* 2007).

Three main Variscan metamorphic-igneous domains are recognized in the Ossa Morena Zone (Portuguese

†Author for correspondence: hsantov@fc.up.pt

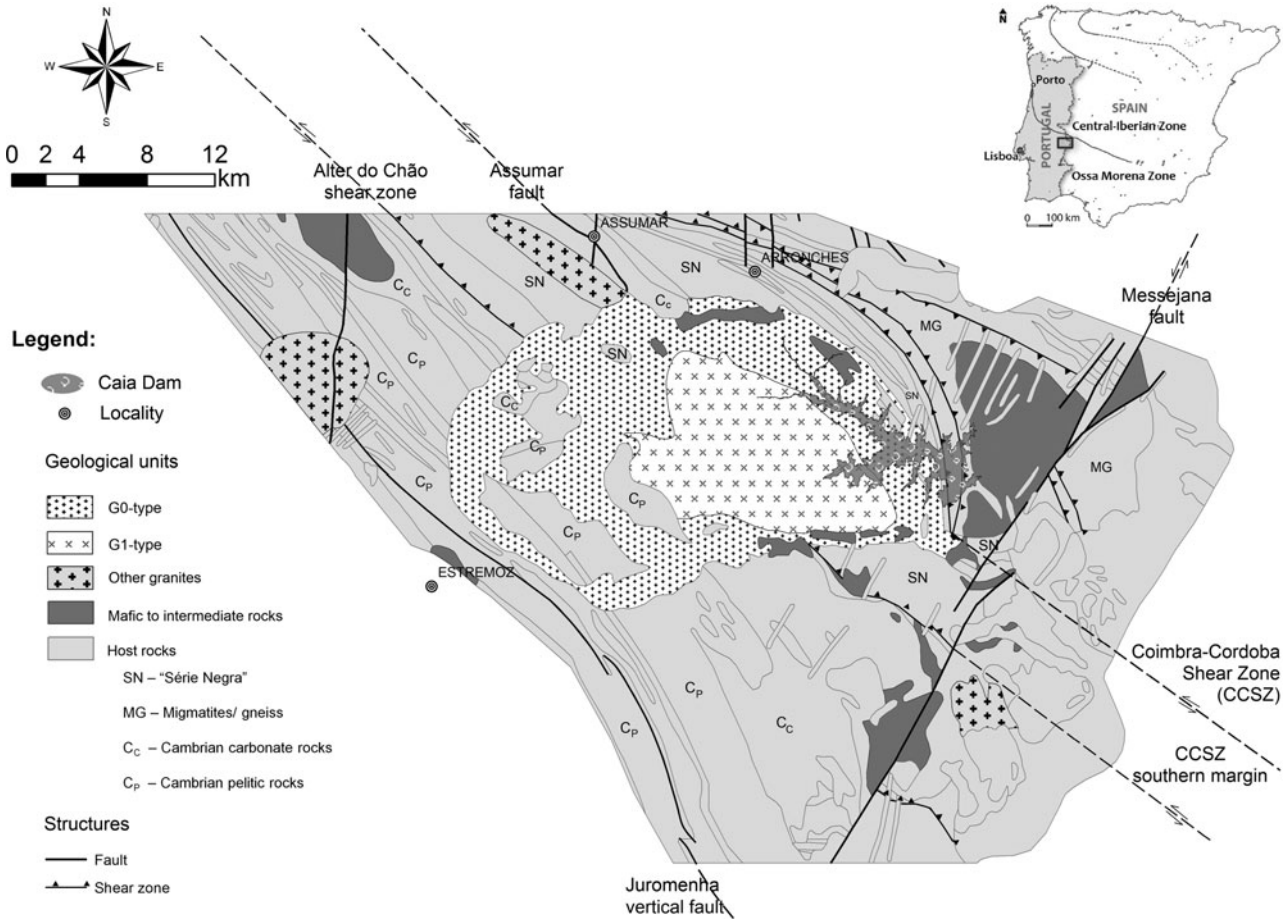

Figure 1. Simplified geological map of the SEPC and its host rocks.

part), from the north to the south: the NE Alentejano Massif; the Évora Massif; and the Beja Igneous Complex (Pereira *et al*. 2007).

The Variscan magmatism from Beja Igneous Complex is typically calc-alkaline with a continental margin arc signature, being directly and indirectly related to the subduction of the Rheic Ocean (e.g. Jesus *et al*. 2007; Pin *et al*. 2008; Lima, 2013). The calc-alkaline plutonic bodies are complex, usually zoned and have small sizes.

The Ossa Morena Zone magmatism from the other metamorphic-igneous domains (NE Alentejano Massif and Évora Massif) is characterized by the appearance of gabbroic rocks associated with basic and acid rocks and to volcanic and subvolcanic events (Sanchez-Carretero *et al*. 1990). The work done by several authors on the magmatism of the Ossa Morena Zone (e.g. Lopes *et al.* 1998; Moita, Santos & Pereira, 2009; Lima, 2013; Pereira *et al*. 2013) has provided good geological mapping, geochemistry and petrography of these granites; however, the relationship between their emplacement and regional tectonics has so far remained unknown.

In this paper the characterization of the magnetic fabric for the Santa Eulália Plutonic Complex (SEPC), located in the NE Alentejano Massif, is carried out as part of a multidisciplinary study to examine the structural patterns of the pluton, the redox conditions of the magma genesis and the role of magma dynamics-related deformation of the Ossa Morena Zone.

The SEPC is a late Variscan granite massif with an elliptical outline intersecting the NW–SE Variscan dominant regional structures in the most northerly sectors of the Ossa Morena Zone. The SEPC is a ring complex composed, from the rim to the core, of a medium- to coarse-grained pink granite (G0-type) with biotite (± hornblende) as the dominant mafic mineral. This composition involves large (kilometre-scale) elongated masses of mafic (gabbroic) to intermediate (granodioritic) rocks, here referred to as the M-group, and a central grey medium-grained granite (G1-type) which is typically biotitic. The latter sometimes shows a slight porphyritic tendency, especially in a few outcrops located near the contact with the peripheral G0-type ring (Lopes, Lopes & Lisboa, 1997; Lopes *et al.* 1998; Menéndez *et al.* 2006).

The petrophysical characterization of the SEPC presented here comprises anisotropy of magnetic susceptibility and isothermal remanent magnetization analyses. These methods have already been applied in Portuguese plutons of the Central Iberian Zone (e.g. Sant'Ovaia *et al*. 2000, 2010; Dória *et al.* 2009; Martins, Sant'Ovaia & Noronha, 2009, 2013; Martins *et al.* 2011). Anisotropy of magnetic susceptibility studies may be used to characterize and measure weak

https://doi.org/10.1017/S0016756814000569 Published online by Cambridge University Press

anisotropic fabrics (foliations and lineations), either magmatic or solid-state. These are essential for describing the fabric of a granite, identifying the constraints leading to the granite intrusion and linking these features to the regional tectonics (e.g. Hrouda, 1982; Borradaile, 1988; Borradaile & Henry, 1997; Bouchez, 1997). Isothermal remanent magnetization analysis provides information about the magnetic carriers. These data are complemented by the study of the microstructures. Since the magnetic fabric provides structural information restricted to the exposure level of the complex, two-dimensional (2D) gravity modelling was also performed to obtain information about the geometry and location of the feeder zones. Finally, in order to understand the microfracturation geometry and the brittle stress constraints, microscopic observations of the geometry of the fluid-inclusion planes and the chemical characterization of the palaeofluid trapped in the healed microcracks from the studied lithologies were made.

2. Geological setting

2.a. General framework

The Santa Eulália Plutonic Complex (SEPC) is a granitic body that occupies an area of 400 km^2 and is located in the northern part of the Ossa Morena Zone of the Variscan Iberian sector, near the limit of the Central Iberian Zone. Available geochronologic Rb–Sr data indicate an age of 290 Ma (Pinto, 1984).

This sector is characterized by a Variscan sinistral transpressive/transtensive tectonic regime; processes that co-existed together occurred separately in neighbouring regions by the means of strain partitioning (Araújo *et al*. 2013) which is materialized by the Coimbra–Cordoba Shear Zone (CCSZ) and associated strike-slip faults, namely Assumar and Alter do Chão structures (Fig. 1).

The SEPC is limited to the northeast by the CCSZ and to the southwest by the Juromenha vertical fault (Araújo *et al*. 2013). The Assumar and Alter do Chão faults separate two structural domains: the blastomylonitic structural domain to the northeast and the São Saturnino – Juromenha domain (e.g Araújo *et al*. 2013; Lopes *et al.* 2013) to the southwest. The blastomylonitic domain is a sinistral transcurrent Variscan shear zone composed of metasedimentary and meta-igneous rocks (e.g. Oliveira, Oliveira & Piçarra, 1991; Araújo *et al*. 2013), slightly deflected by the SEPC. The São Saturnino – Juromenha structural domain corresponds to a NW–SE-directed shear zone which preserves a complex sequence of transtensive and transpressive events (Lopes *et al*. 2013). To the east, the SEPC is limited by a major NNE–SSW-oriented tectonic structure known as the Messejana fault. This fault has a complex tectonic history, as an initial late Variscan left-lateral strike-slip fault later reactivated as a transtensional fault allowing the emplacement of Triassic–Jurassic magmas (Schermerhorn *et al*. 1978).

The host rocks of the SEPC are composed of upper Proterozoic – lower Palaeozoic low- to high-grade metamorphic rocks. East of the SEPC, the host rocks are metasedimentary siliciclastic with black cherts of Ediacaran age referred to as 'Série Negra', and some intercalations of alkaline rocks. This low-grade unit is adjacent to a high-grade unit with migmatites and gneiss to the northeast. In the north, south and west of the SEPC, a low-grade metasedimentary and metavolcanic Cambrian sequence is composed of quartz-pelitic, carbonate and volcanic rocks. The roof pendants, spatially associated with G0-type rocks, show internal structure and lithological diversity consistent with the external metasedimentary and meta-igneous units.

To both the east and west, the host rocks comprise phyllite and quartz-phyllite in chlorite zone conditions without any thermal effects, even at a short metric distance from the contact. Further, the Cambrian carbonate rocks cropping out in narrow bands near the ESE border of SEPC do not show any post-kinematic thermal effect. The igneous and meta-igneous rocks (granites, migmatites, gneiss, gabbros, hyper-alkaline rocks, basic and acid volcanite) do not present thermal effects as expected, because these rocks are mineralogically and texturally stable at high temperatures. Unlike in the western sector of SEPC, the thermal effects are well marked in the metasedimentary roof pendants by metamorphic and metasomatic paragneisses in pelitic and carbonate hornfels. The latter show large wollastonite crystals (Dória *et al*. 2011; Cruz, Ribeiro & Sant'Ovaia, 2013; Ribeiro, Cruz & Martins, 2013).

2.b. Major and trace element geochemistry

The SEPC has two main granites which present different compositions and textures, exhibiting gradual contacts in the field. From the rim to the core, this ring plutonic complex is composed of G0 involving the M-group rocks, then passes to G1, the central grey monzonitic granite (Fig. 1).

Elemental geochemistry confirms important differences between M, G1 and G0 types. The mafic to intermediate rocks of the M-group (olivine gabbros to granodiorites) are metaluminous and present wide compositions: 3.34–13.51 wt % MgO; 0.70–7.20 ppm Th; 0.84–1.06 Eu* (chondritic normalized values between Sm and Tb). The G1-type are typically monzonitic granites with a slight peraluminous character and represent the less evolved granitic rocks: 0.65–1.02 % MgO; 13.00–16.95 ppm Th; and 0.57–0.70 Eu*. The G0 granites are the most evolved magmatic rocks of the SEPC with a dominant metaluminous character and strongly differentiated compositions: 0.00–0.62 MgO; 15.00–56.00 Th; and 0.19–0.42 Eu*. According to SiO_2 v. ($Na_2O + K_2O$–CaO) relationships (e.g. Frost *et al.* 2001; Frost & Frost, 2011) the SEPC shows a calc-alkaline character, but a few samples of the G0 group reach the alkali-calcic field. On the basis of SiO_2 v. $FeO^t/(FeO^t + MgO)$ correlation (Fig. 2), the SEPC

https://doi.org/10.1017/S0016756814000569 Published online by Cambridge University Press

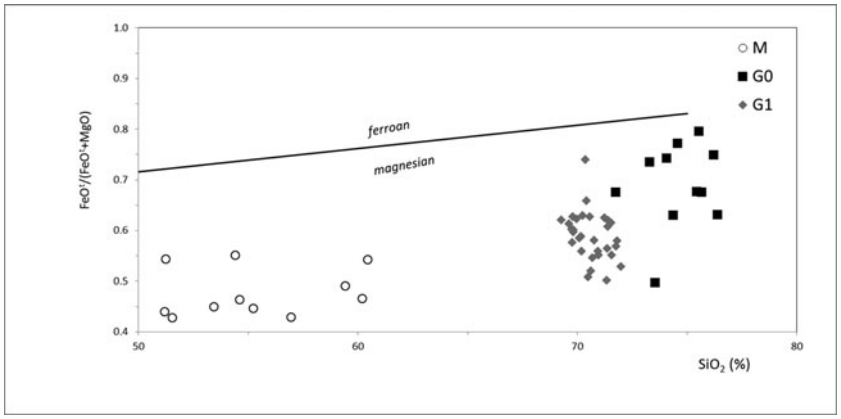

Figure 2. SiO2 v. FeO^t/(FeO^t/MgO) discriminant diagram for SEPC representative samples.

(M–G1–G0) plutonic association should be classified as magnesian (Frost *et al.* 2001; Frost & Frost, 2011).

2.c. Petrography and microstructures

In the G0-type the main mineral assemblage observed includes quartz (26–39 %), K-feldspar (36–53 %), plagioclase (13–28 %), biotite (5–19 %) and amphibole (<2 %). As accessory minerals, allanite, zircon and sphene are present. Quartz occurs as anhedral to subhedral grains. The biotite appears partially to completely chloritized with pleochroic halos of associated zircon and sphene. The plagioclases occur as altered megacrystals with a well-marked zonation. Myrmekitic intergrowths are common in the borders of plagioclases when in contact with K-feldspar. The K-feldspar, perthitic orthoclase and microcline occur as heterogranular crystals. Microcline also occurs as interstitial crystals with well-developed twins. The albitization of feldspar is common either inside the crystals or in their borders. The amphibole is hornblende and presents a chlorite alteration. The microstructures observed are quartz subgrain boundaries, sometimes folded biotites and occasionally bent plagioclase twin planes.

As the main mineralogical assemblage, the G1-type contains quartz (22–33 %), plagioclase (29–40 %), K-feldspar (16–27 %), biotite (6–15 %) and muscovite (2–16 %). As accessory minerals, zircon and apatite are present. The quartz grains are anhedral and with a slight deformation. The biotite is partially to fully chloritized and presents zircon pleochroic halos. The K-felsdpar is orthoclase, generally perthitic and microcline. The muscovite is more frequent when compared to the G0-type and increases toward the centre of the SEPC. The plagioclase shows alteration, sericitization, is zoned and presents myrmekites. Another characteristic of the G1-type is the greater amount of plagioclase in relation to the K-feldspar when compared to the G0-type. As microstructures, the rare undulatory extinction in quartz grains is evident.

For textures observed in thin-sections of the G0 (Fig. 3a–e) and the G1 (Fig. 3f–h) granites which are essentially magmatic to submagmatic, the biotite is undeformed (Fig. 3f, h) and undulatory extinctions in quartz are rare or absent (Fig. 3g). However, the presence of bending of biotite cleavages (Fig. 3e) and of plagioclase twin planes (Fig. 3d), as well as quartz subgrains boundaries (Fig. 3b, c), in the G0-type can be interpreted as the result of a stronger deformation of the G0, although in a submagmatic state.

Gabbro-diorite rocks from the M-group are evident as the main mineralogical assemblage includes plagioclase, amphibole (hornblende), orthopyroxene, clinopyroxene, biotite and epidote. In the M-group granodiorite rocks, the assemblage plagioclase, potassic feldspar, quartz, amphibole, biotite and epidote prevails.

3. Petrophysical studies

3.a. Sampling

At each site, four oriented cores (25 mm in diameter and 60–70 mm in length) were collected *in situ* with a portable drill machine. Each core was sawed into two (eventually three) 22-mm-long specimens. At least eight specimens per station were obtained for magnetic measurements.

This study was based on 637 rock cylinders from 76 sampling sites roughly distributed throughout the SEPC and also in the host rocks: 29 sites in G0-type; 27 in G1-type; 5 in the M-group; and 15 in roof pendants and host rocks (Fig. 4).

3.b. Anisotropy of magnetic susceptibility and isothermal remanent magnetization analytical techniques

The relationship between the magnetization induced in a material M and the external field H is defined as $M = kH$, where k is the magnetic susceptibility. Because M (per unit volume) and H have the same units (A m^{-1}), k is dimensionless. If the material is anisotropic, magnetic susceptibility is represented by a second-order symmetric tensor known as the anisotropy of magnetic susceptibility tensor (Graham, 1954; Hrouda, 1982;

https://doi.org/10.1017/S0016756814000569 Published online by Cambridge University Press

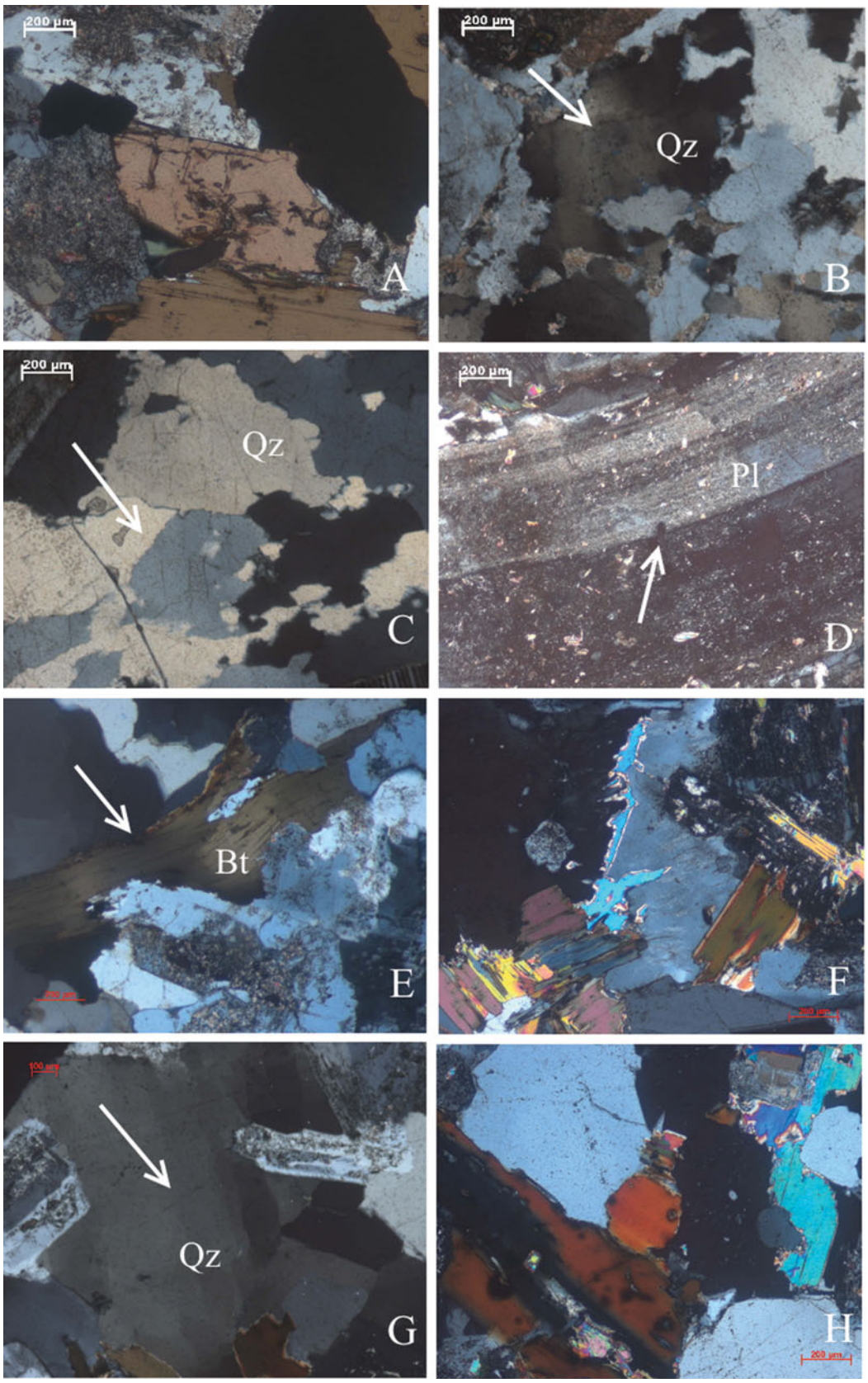

Figure 3. (Colour online.) Mineralogy and microstructures observed in (A–E) facies G0 and (F–H) G1. All photomicrographs under crossed polars. (B, C) Subgrain boundaries in quartz; (D) bent plagioclase twins; (E) bent biotite clivages; and (G) rare undulatory extinction in quartz grains.

https://doi.org/10.1017/S0016756814000569 Published online by Cambridge University Press

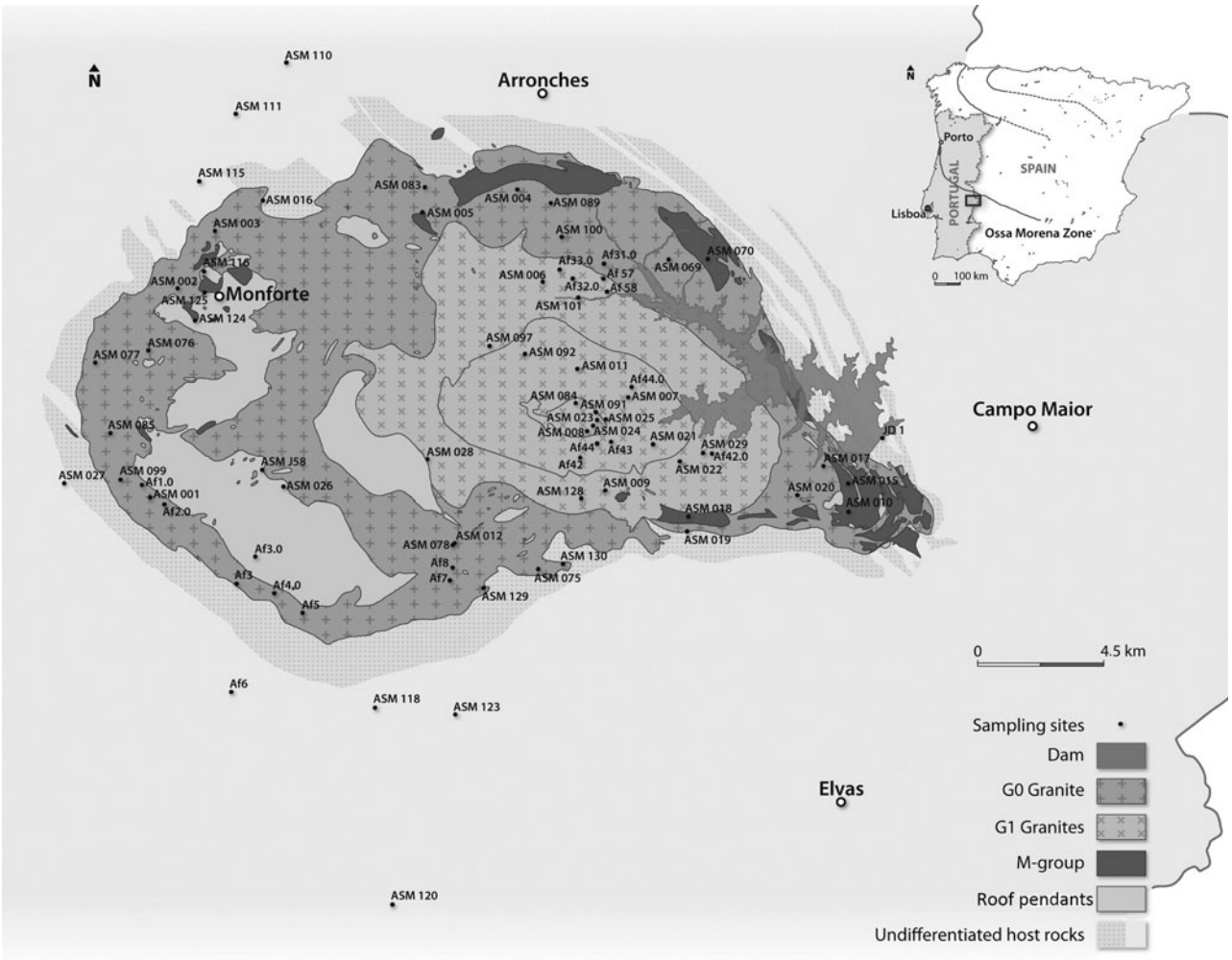

Figure 4. Sampling sites for AMS and IRM studies.

Collinson, 1983; Bouchez, 1997). The magnetic susceptibility reflects the mineral composition of the rock which can have a diamagnetic (e.g. quartz or feldspar), paramagnetic (e.g. biotite, muscovite or hornblende) or a ferromagnetic behaviour (e.g. magnetite or hematite).

Anisotropy of magnetic susceptibility (AMS) measurements were performed using KLY-4S Kappabridge susceptometer Agico model (Czech Republic) from the Centro de Geologia of Porto University. For each site, the ANISOFT 4.2 program package (www.agico.com) enabled us to calculate the mean susceptibility K_m, which is the mean of the eight (or more) individual arithmetic means $(k_1 + k_2 + k_3)/3$. Also calculated were the intensities and orientations of the three axes $K_1 \geq K_2 \geq K_3$, which are the tensorial means of the $k_1 \geq k_2 \geq k_3$ axes for the eight specimens, and the 95 % confidence angles E_{12}, E_{23} and E_{31} corresponding to these three axes.

The magnetic fabric is defined by the magnetic lineation (parallel to the long axis of the mean ellipsoid orientation average, K_1) and the magnetic foliation (plane perpendicular to the orientation of K_3, the short axis). The degree of magnetic anisotropy P (%) corresponds to $[(K_1/K_3)–1]\times 100$. To describe the shape of the anisotropy of magnetic susceptibility ellipsoid, the shape parameter T is defined (Jelinek, 1981)

$$T = 2\frac{\ln(K_2/K_3)}{\ln(K_1/K_3)} - 1.$$

The remanence acquired by a sample exposed to a direct magnetic field at ambient temperature is referred to as isothermal remanent magnetization (IRM). The IRM acquisition curves are important to estimate the characteristic coercivity of ferromagnetic minerals. The trend of the acquisition curves depends on the relative concentration of low-coercivity magnetite-type minerals and high-coercivity hematite-type minerals.

The IRM values were measured using a Molspin magnetometer and fields were imparted using a Molspin pulse magnetizer at the University of Coimbra. Samples were magnetized first in the same direction and second in the opposite direction from 12.5 mT up to 1 T. The IRM at 1 T is defined as the saturation isothermal remanent magnetization (SIRM).

https://doi.org/10.1017/S0016756814000569 Published online by Cambridge University Press

3.c. Anisotropy of magnetic susceptibility results

3.c.1. Bulk susceptibility, anisotropy degree and shape parameter

The K_m values range between 30.3 and 18672.0×10^{-6} SI for all rocks (Table 1). Two major groups can be established: G0-type, with $41.6 < K_m < 7343.7\times10^{-6}$ SI (mean 1357.4×10^{-6} SI) and G1-type with $55.1 < K_m < 133.7\times10^{-6}$ SI (mean 97.0×10^{-6} SI).

In basic rocks from the M-group K_m values are homogeneous, ranging between 606.4 and 834.3×10^{-6} SI with a mean of 620.9×10^{-6} SI (Fig. 5). In the roof pendants and host rocks, K_m values range between 55.9 and 717.8×10^{-6} SI; the wide variation is due to the different composition of these rocks.

The magnetic anisotropy P ranges between 1.5 and 18.7 % for G0-type (mean 6.2 %) and between 1.3 and 8.4 % in the central granite G1 (mean 3.1 %). G0-type has the highest anisotropy degree (Fig. 6). The ellipsoid shape T ranges between –0.354 and 0.768 in all granitic types, with the strongest oblate ellipsoids in G1 (mean 0.365) and slightly oblate in G0 (mean 0.099) (Fig. 7). The prolate ellipsoids are mainly present on the G0 samples in the east, NW and SE borders. In the M-group T values have a wide range and P values are between 1.0 % and 5.9 % (Fig. 7). Finally, in host rocks and roof pendant rocks, T and P values have a wide range due to the large variety of lithologies included in this group.

3.c.2. Magnetic fabric patterns

The magnetic fabric (lineation and foliation) is generally parallel to the mineral fabric in paramagnetic granites (Heller, 1973; Tarling & Hrouda, 1993; Bouchez, 1997). The exception is minerals, which present an inverse magnetic fabric (e.g. cordierite). In the studied granites that display magmatic to submagmatic microstructures, the magnetic foliation and lineation are markers of the flattening and stretching, respectively, of the magmas in the latest stages of their emplacement.

In G0 the magnetic foliations are concentrically distributed with inwards steep dips. In the east part of the SEPC (in G0) magnetic foliations are dominantly ENE–WSW-striking. The mean foliation orientation is N73E, 76SE (Fig. 8; see also stereograms of the three axes of the AMS ellipsoid in the online Supplementary Material available at http://journals.cambridge.org/geo). In G1 the magnetic foliations have outwards steep dips and are NE–SW to ENE–WSW-striking, displaying a dome-like structure. In G1 the mean foliation orientation is N72E, 78SE (Fig. 8).

The magnetic lineations in G0 (Fig. 9; see also stereograms of the three axes of the AMS ellipsoid in the online Supplementary Material available at http://journals.cambridge.org/geo) have a distinct behaviour over the pluton: magnetic lineations are subvertical in the eastern sector and they plunge *c.* 50° to the SW in the western sector. In G1 (Fig. 9), magnetic lineations are scattered in orientation but always plunging moderately.

In the M-group magnetic foliations are dominantly NE-striking and lineations are scattered with steep dips. Mean foliations and lineations were not calculated due to the reduced number of sampling sites.

In host rocks and roof pendant rocks, magnetic foliations are NW–SE-striking (mean N138E, 82NE) underlying the Variscan dominant regional structures and magnetic lineations have steep plunges to the northwest.

3.c.3. Thermomagnetic curves

In order to identify different ferromagnetic contributions, thermomagnetic experiments were performed in low field with a CS-2 furnace apparatus attached to the KLY-3 susceptometer (Laboratoire des Mécanismes et Transferts en Géologie, Université Toulouse). Samples consist of fragments obtained from four rock specimens (G0 ASM76, ASM77 and ASM85 and G1 Af57). The samples were subjected to increasing temperatures up to 700 °C. Thermomagnetic experiments performed on samples ASM76 and ASM77 (G0) show a significant fall of magnetic susceptibility at 580 °C, which indicates the presence of magnetite (Fig. 10a). On Af57 (G1) and ASM85 (G0), magnetic susceptibility decreases regularly with increasing temperature, typical of a paramagnetic behaviour; there is also a slight fall around 580 °C, indicating the presence of a small quantity of magnetite (Fig. 10b).

3.d. Isothermal remanent magnetization results

The saturation isothermal remanent magnetization values range from 0.789 to 51.762 A m^{-1} (mean 9.345 A m^{-1}, $N = 16$) in G0 and between 0.005 and 0.043 A m^{-1} (mean 0.027 A m^{-1}, $N = 13$) in G1 granites (Table 2). In the M-group, the SIRM values range between 0.580 and 5.657 A m^{-1} (mean 2.634 A m^{-1}, $N = 5$). In host rocks and roof pendant rocks, the values are widely dispersed between 0.062 and 20.776 A m^{-1} (mean 3.638 A m^{-1}, $N = 6$).

In G0 granites, the acquisition curves show saturation in fields between 300 and 400 mT followed by a small increase in intensity with increasing fields. In G1-type, the acquisition curves show that saturation is not obtained at the applied fields. In the M-group, the curves are similar to G0 (Fig. 11). In host rocks and roof pendant rocks, the curves show different shapes with saturation in fields of 300–400 mT for some samples and with no saturation in others.

The ratio of the saturation isothermal remanent magnetization to the mean magnetic susceptibility (SIRM/K_m) has values of 7.119, 0.298, 3.425 and 7.925 kA m^{-1} for G0, G1, M and host and roof pendant rocks, respectively.

https://doi.org/10.1017/S0016756814000569 Published online by Cambridge University Press

Table 1. AMS data for the sampling sites. K_m – mean magnetic susceptibility in 10–6 SI; P– anisotropy degree; T – shape parameter; Dec, Inc – declination, inclination; E12, E23 and E31 – 95 % confidence angles corresponding to the three axes; N – number of specimens; *: – discarded measurement; ** – not enough data.

Sampling sites	Lithology	K_m ($\times 10^{-6}$ SI)	P (%)	T	K_1 Dec	K_1 Inc	K_3 Dec	K_3 Inc	Foliation	E_{12}	E_{23}	E_{31}	N
ASM 005	M-group	834.3	5.9	0.363	110	77	294	13	N024, 77SE	8	10	4	12
ASM 010	M-group	532.8	1.0	– 0.284	314	11	50	24	N140, 66SW	8	12	5	6
ASM 015	M-group	664.8	4.7	0.519	309	26	90	70	NS, 20W	33	4	5	7
ASM 070	M-group	606.4	1.9	– 0.127	239	13	130	55	N040, 35NW	25	17	9	7
ASM 018	M-group	466.3	2.4	– 0.073	46	42	161	25	N071, 65NW	9	4	3	7
Af3.0Maf	Roof pendants	450.7	7.9	0.178	37	43	238	45	N148, 45NE	10	4	2	7
ASM 026	Roof pendants	717.8	1.3	– 0.356	235	8	346	68	N076, 22SE	13	27	3	8
ASM J58	Roof pendants	290.8	1.9	0.447	*	*	204	33	N114, 57NE	**	**	**	3
ASM 116	Roof pendants	239.9	4.4	0.215	178	74	339	15	N069, 75SE	30	22	26	8
ASM 125	Roof pendants	139.9	0.8	0.151	83	52	331	16	N061, 74SE	12	10	6	8
ASM 124	Roof pendants	332.3	1.5	0.622	234	63	120	6	N030, 84NW	15	5	4	11
Af6.0Enc	Host rocks	474.8	7.7	0.455	325	49	57	2	N147, 88SW	4	4	2	8
ASM 027	Host rocks	364.8	18.3	0.478	317	48	47	0	N137, 90	**	**	**	3
ASM JD1	Host rocks	30.3	6.1	– 0.359	256	14	351	20	N081, 70SE	**	**	**	3
ASM 110	Host rocks	192.6	13.1	0.312	303	42	202	12	N112, 78NE	15	6	8	8
ASM 111	Host rocks	432.1	2.8	0.487	279	46	31	19	N121, 71SW	30	12	5	8
ASM 115	Host rocks	189.4	5.1	– 0.084	155	16	62	10	N152, 80SW	6	30	5	8
ASM 120	Host rocks	14623.8	5.3	0.050	130	53	243	17	N153, 73NE	9	5	1	8
ASM 123	Host rocks	18672.0	12.7	0.532	3	18	264	25	N174, 65NE	7	4	3	6
ASM 118	Host rocks	55.9	2.5	0.481	159	4	250	13	N160, 77NE	39	5	3	8
Af1.0G0	G0	603.6	4.5	0.232	66	63	265	25	N175, 65E	36	35	20	8
Af2.0G0	G0	642.2	5.0	0.117	65	45	240	45	N150, 45NE	40	43	22	8
Af3G0	G0	41.6	4.1	0.237	317	9	59	54	N149, 36SW	35	14	10	8
Af4.0G0	G0	162.1	1.5	0.145	229	7	312	22	N042, 68SE	31	45	9	8
Af5G0	G0	80.4	4.1	– 0.023	305	19	136	70	N046, 20NW	72	41	36	6
Af7G0	G0	816.2	10.1	– 0.033	212	45	306	4	N036, 86SE	5	17	8	8
Af8G0	G0	5437.3	15.2	– 0.144	205	29	353	57	N083, 33S	6	3	4	8
Af31G0	G0	253.5	3.9	– 0.055	294	70	182	8	N092, 82N	36	13	11	15
ASM 001	G0	93.1	4.2	– 0.184	118	19	232	40	N142, 50NE	**	**	**	4
ASM 002	G0	1165.6	3.5	– 0.188	159	69	20	16	N110, 74SW	23	27	18	5
ASM 003	G0	878.8	4.2	– 0.184	171	70	349	18	N079, 72SE	**	**	**	4
ASM 004	G0	1179.3	6.0	0.290	5	81	191	9	N100, 81NE	8	38	6	5
ASM 012	G0	7343.7	18.7	– 0.065	232	39	349	30	N079, 60SE	4	14	6	6
ASM 016	G0	82.7	3.9	0.430	227	52	350	23	N080, 67SE	**	**	**	4
ASM 017	G0	1582.6	5.6	– 0.020	110	69	349	15	N079, 75SE	**	**	**	4
ASM 020	G0	229.4	3.2	0.335	104	72	332	12	N062, 78SE	30	14	7	7
ASM 069	G0	2075.8	8.1	0.237	38	71	191	10	N101, 80NE	**	**	**	4
ASM 075	G0	357.0	4.3	0.107	201	33	313	29	N043, 61SE	15	10	14	9
ASM 076	G0	2028.8	6.9	0.103	275	29	10	9	N100, 81S	42	14	12	9
ASM 077	G0	2433.0	8.1	– 0.006	104	63	314	24	N044, 60SE	44	43	26	13
ASM 078	G0	3709.3	11.9	– 0.272	213	15	83	68	N173, 22W	5	17	3	13
ASM 083	G0	707.1	5.5	0.068	106	61	331	21	N061, 69SE	7	6	3	8
ASM 085	G0	126.9	3.2	– 0.060	94	29	208	37	N118, 53NE	45	32	29	11
ASM 089	G0	4448.8	11.7	0.683	86	47	342	13	N072, 77SE	26	30	6	10
ASM 099	G0	71.5	4.6	0.158	52	42	309	14	N039, 76SE	70	44	41	11
ASM 100	G0	766.9	7.9	0.076	310	68	41	1	N131, 89SW	32	61	20	11
ASM 129	G0	840.7	2.6	0.290	63	15	154	7	N084, 83NW	18	9	7	11
ASM 130	G0	987.9	3.0	0.238	237	53	143	3	N053, 87NW	39	14	13	11
ASM 019	G0	219.2	3.3	0.374	156	80	337	10	N067, 80SE	36	8	18	6
ASM 128	G1	91.6	3.3	0.486	107	3	16	19	N106, 71SW	6	14	5	9
Af32.0G1	G1	106.8	8.4	0.263	40	16	221	74	N131, 16NE	40	26	5	16
Af33.0G1	G1	94.9	6.2	0.598	314	51	175	32	N085, 58N	32	19	15	15
Af57G1	G1	88.1	3.5	0.575	90	19	191	30	N101, 60N	48	5	4	15
Af58G1	G1	96.5	3.4	0.448	118	9	27	2	N117, 88SW	19	10	7	16
ASM 006	G1	94.4	4.3	0.337	300	45	184	24	N094, 66N	12	5	4	6
ASM 009	G1	94.0	2.8	0.385	238	25	332	7	N062, 82SE	26	21	33	7
ASM 022	G1	93.7	4.0	0.062	183	64	335	23	N065, 67SE	2	7	1	6
ASM 028	G1	86.0	2.0	0.300	206	57	10	32	N100, 58SW	26	7	5	7
ASM 029	G1	88.9	3.1	0.566	59	32	326	12	N056, 78SE	2	5	5	6
ASM 097	G1	87.9	4.1	0.201	303	33	165	49	N75, 41NW	21	42	5	9
ASM 101	G1	86.0	3.4	0.768	104	3	195	26	N105, 64NE	53	6	5	12
Af42.0G2	G1	97.1	3.8	0.106	356	79	180	11	N090, 79N	14	8	9	5
Af42G2	G1	109.0	2.4	0.478	217	41	36	49	N126, 41SW	17	70	8	8
Af43G2	G1	107.4	2.2	0.427	145	39	291	46	N021, 44E	21	7	5	12
Af44G2	G1	119.7	2.4	0.600	192	30	314	44	N044, 46SE	34	4	4	10
Af44.0G2	G1	104.6	2.8	0.349	40	41	230	49	N140, 41NE	21	10	8	15
ASM 007	G1	108.3	2.3	0.517	207	31	11	58	N101, 32SW	21	13	6	7
ASM 008	G1	118.3	2.3	0.488	169	51	309	32	N039, 58SE	21	9	5	7

https://doi.org/10.1017/S0016756814000569 Published online by Cambridge University Press

Table 1. Continued.

Sampling sites	Lithology	K_m ($\times 10^{-6}$ SI)	P (%)	T	K_1 Dec	K_1 Inc	K_3 Dec	K_3 Inc	Foliation	E_{12}	E_{23}	E_{31}	N
ASM 011	G1	110.8	1.8	0.282	274	22	69	66	N159, 24SW	26	15	7	6
ASM 021	G1	133.7	1.8	0.260	141	48	298	38	N028, 52SE	16	13	6	8
ASM 025	G1	93.9	2.6	−0.015	2	2	272	23	N002, 67E	4	17	6	11
ASM 84	G1	69.7	2.9	0.682	250	29	145	25	N055, 65NW	23	9	4	8
ASM 91	G1	100.0	1.3	−0.354	1	59	113	13	N023, 77NW	9	63	10	10
ASM 92	G1	117.6	2.3	0.568	40	38	172	41	N082, 49N	9	6	4	9
ASM 023	G1	55.1	2.8	0.252	187	21	305	38	N035, 52SE	52	19	12	8
ASM 024	G1	65.9	2.8	0.230	63	24	316	32	N046, 58SE	65	8	7	7

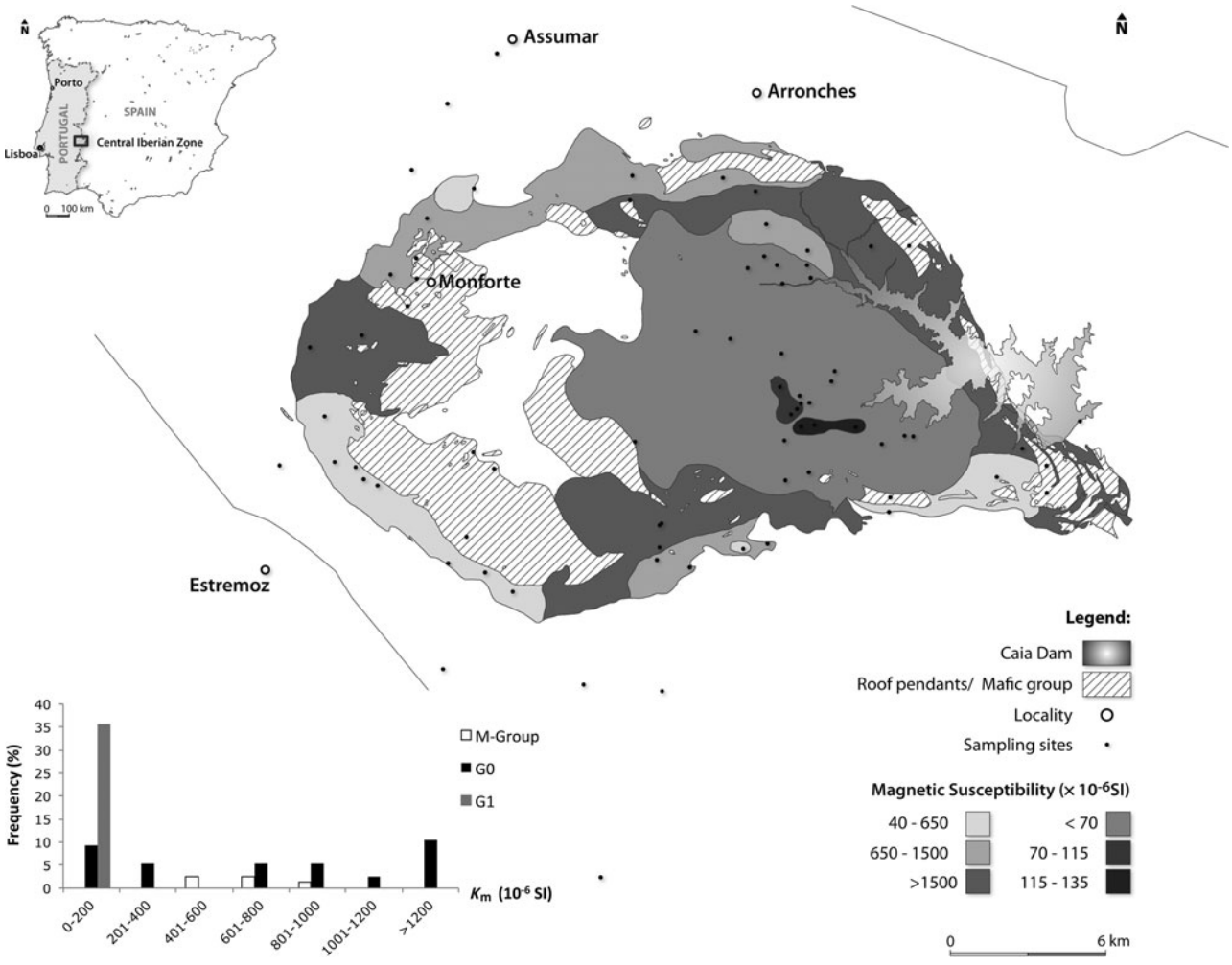

Figure 5. Map of the magnetic susceptibility (K_m) and histogram of the bulk susceptibility values.

4. Gravity study

An east–west gravity profile obtained using a Worden Prospector gravimeter with a precision of 0.02 mGal was performed over 76 closely spaced (500 m) stations.

Altitudes were determined using a differential GPS. The data were corrected for the intrinsic constant of the apparatus and for the usual topography, latitude and elevation corrections. The Bouguer correction was performed assuming a density of 2.70. Densities were measured using cylindrical specimens that were collected for the anisotropy of magnetic susceptibility study. The densities of the G0 and G1 types were calculated as 2.56 and 2.60, respectively, contrasting with an average density of 2.70 for the host rocks. The analysis of the Bouguer anomaly allowed us to model the 2D shape of the SEPC along the profile. To constrain the gravity model, the cropping out limits of the SEPC were used.

4.a. Two-dimensional gravity modelling

The G0-type in western part of the profile presents an almost flat footwall with a depth of *c.* 2.5 km. The gravimetric profile is steep in the vicinity of the contact with the G1-type. The profile indicates that the feeder zone of the SEPC must be located in the

https://doi.org/10.1017/S0016756814000569 Published online by Cambridge University Press

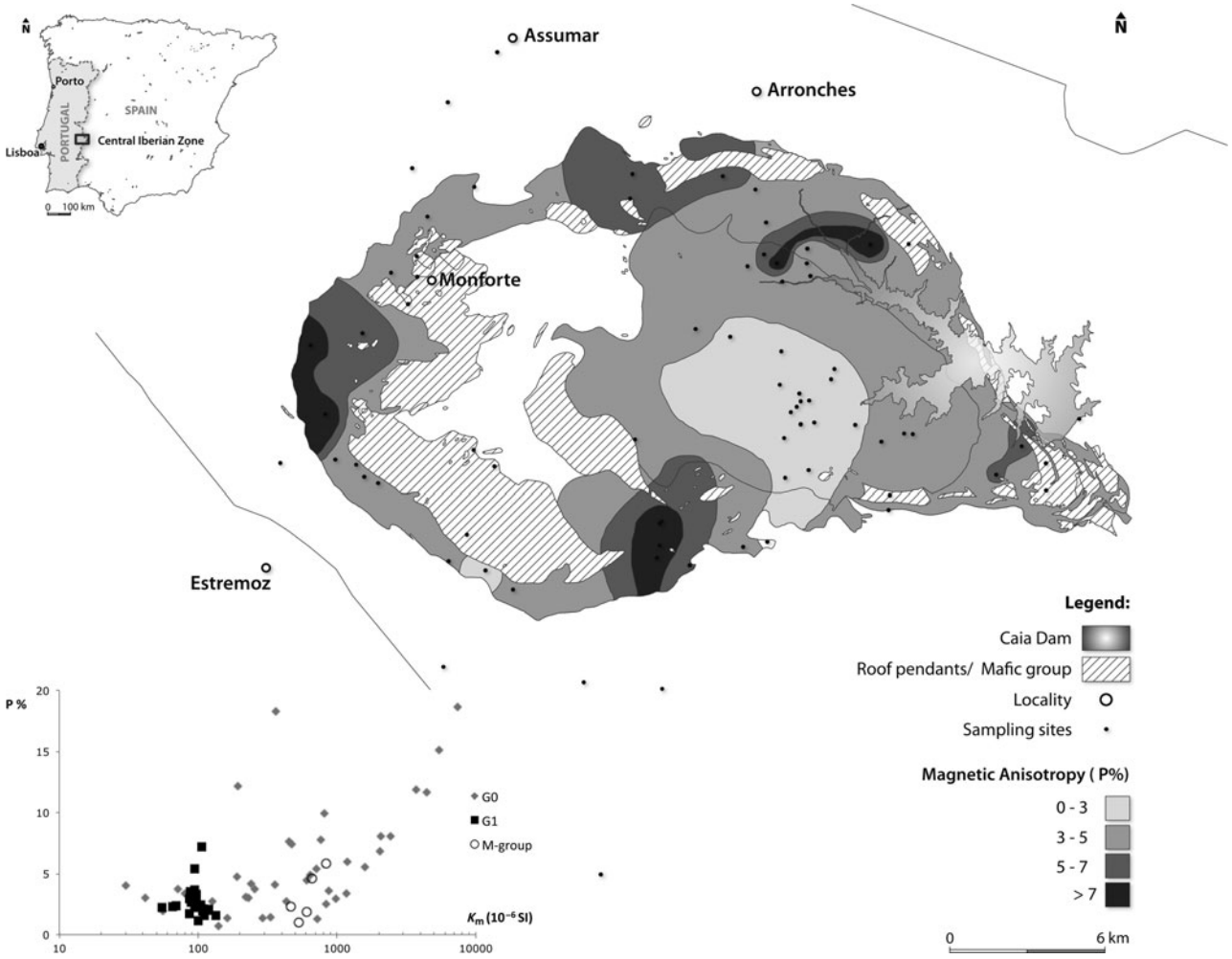

Figure 6. Map of the anisotropy of magnetic susceptibility *P* and correlation between bulk susceptibility and magnetic anisotropy.

eastern part, overlapping with the probable position of the Alter do Chão shear zone which does not crop out at the present-day erosion level (Fig. 12). The eastern part of the gravimetric profile has a steeper shape, indicating the probable conditioning of the feeder zone by the Messejana fault. The modelling of the gravimetric data allows us to define a minimum depth for the feeder zone of the SEPC of *c.* 7.5 km.

5. Fluid inclusion planes studies

Fluid inclusion planes result from the healing of former open cracks and appear to be fossilized fluid pathways (e.g. Roedder, 1984; Lespinasse & Pecher, 1986; Lespinasse, 1999). The fluid inclusion planes occur in sets and are formed as mode-I cracks materializing the $\sigma_1-\sigma_2$ plane (Lespinasse & Cathelineau, 1995). Their study provides valuable information about local stress in rocks (Lespinasse & Pecher, 1986) as well as allowing the relationships between tectonic events and fluid percolations to be established.

A total of eight oriented subvertical rock cylinders from SEPC which were used for the AMS studies were chosen and 200 μm doubly polished wafers, cut perpendicular to the cylinders, were prepared. The strike of the fluid inclusion planes was determined on oriented thick sections (related to geographic north) using an image analyser attached to a transmitted light microscope. In each thick section *c.* 100 planes were measured. The image acquisition and analysis and the mapping of the fluid inclusion planes was performed using the software GeoImagin (http://home.uevora.pt/~pmn/geoimagin/).

Fluid inclusion planes were only studied in quartz since this mineral has a rapid rate of healing (Smith & Evans, 1984; Brantley, 1992), easily trapping fluids as fluid inclusions, which enables a clearer visualization of the microcracks.

Fluid inclusion petrography and microthermometric characterization of the fluids were carried out using a Chaixmeca heating-freezing stage for criometry (Poty, Leroy & Jachimowicz, 1976) and a Linkam stage for thermometry (Shepherd, Rankin & Alderton, 1985). The stages were calibrated with a melting point of natural and synthetic fluid inclusions at $T<0$ °C and with manufactured standards Merck Co. Schemlzkorper at $T>30$ °C. The analytical precision was of ± 0.1 °C and ± 1 °C in criometry and thermometric studies, respectively. The degree of fill, F_{lw} (volume of liquid phase/total volume) was estimated at room temperature by reference to the volumetric charts of Roedder (1984) and Shepherd, Rankin & Alderton (1985).

https://doi.org/10.1017/S0016756814000569 Published online by Cambridge University Press

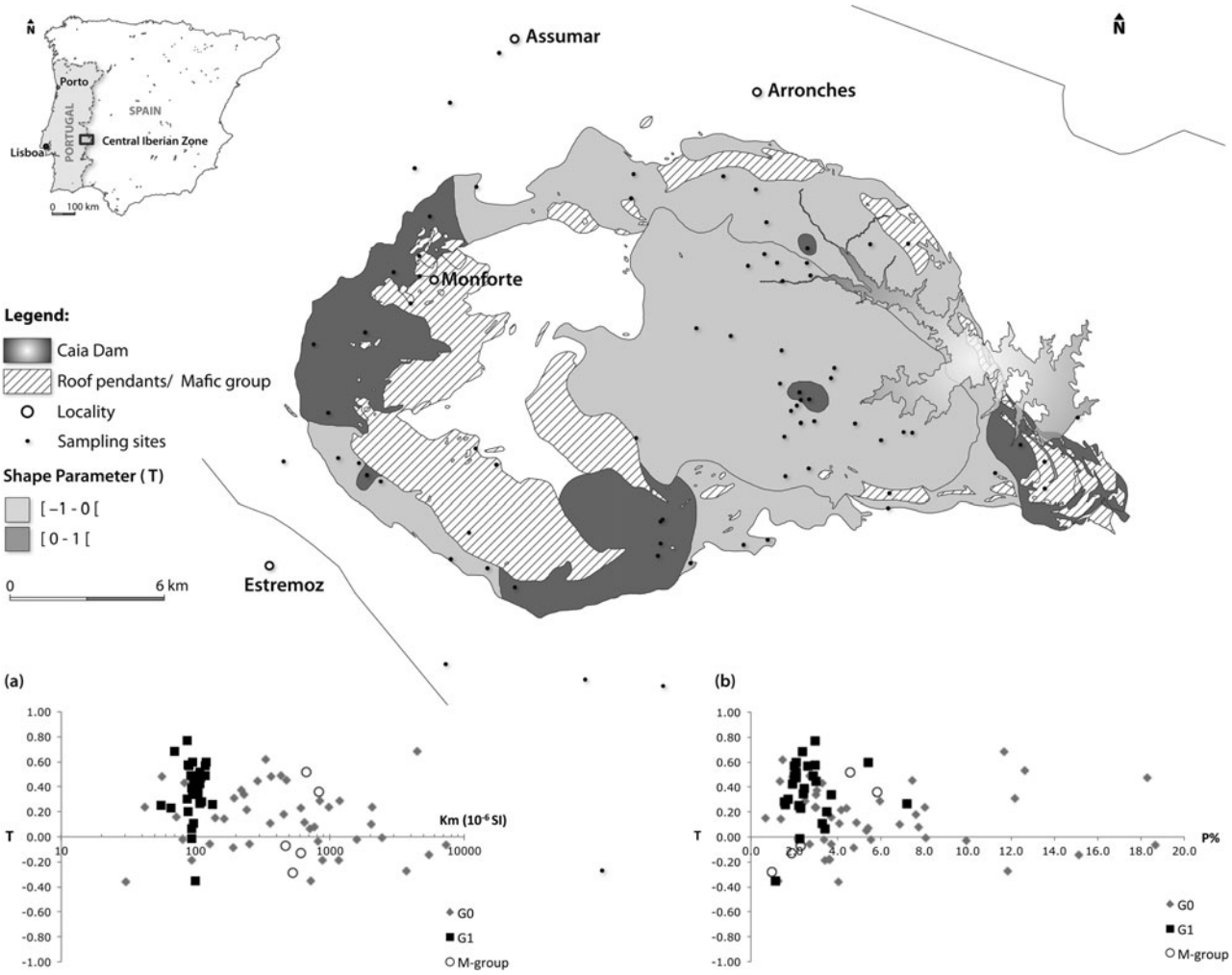

Figure 7. Map of shape parameter *T* and correlations with (a) bulk susceptibility; and (b) magnetic anisotropy.

Aqueous fluid salinities, expressed in wt % equivalent (eq.) NaCl, were calculated using the melting temperature of the ice and the equation of Bodnar (1993). In aqueous carbonic inclusions, the melting temperature of clathrates and the software developed by Bakker (2003) were used. Molar fractions of CO_2 and N_2 species were determined in the volatile phase of individual fluid inclusions by Raman analysis performed on a Labram Dilor Jobin Yvon Spex Raman spectrometer coupled to an Olympus optical microscope. The different fluid species were quantified via specific procedures (Prieto *et al.* 2012).

Samples Af31.0, ASM020, ASM001 and ASM004 (G0-type) and ASM006, ASM097, ASM092 and ASM007 (G1-type) were selected from the SEPC for the fluid inclusion planes studies.

Figure 13 depicts rose diagrams showing the fluid inclusion plane directions for each granite type. The analysis of the rose diagrams shows that the G0-type quartz contains fluid inclusion plane sets with a well-expressed NW–SE preferential orientation, and for G1-type the NNE–SSW to NE–SW direction becomes predominant (Fig. 13).

Three samples – Af31.0 and ASM020 (G0) and ASM097 (G1) – were selected for the fluid inclusion characterization. Three main fluid inclusion types (aqueous carbonic, aqueous with low–moderate salinities and aqueous with high salinities) were observed, based on number of phases at room temperature and their phase behaviour on cooling.

5.a. Aqueous carbonic fluids

Aqueous carbonic fluid inclusions were only recorded in the sample ASM020 from G0-type. They are mostly three-phase inclusions (liquid H_2O + liquid CO_2 + CO_2 vapour) at room temperature. They generally display dimensions within the range 6–20 μm. The melting temperature of the CO_2 (T_m CO_2) was observed to be between –59.7 and –56.7 °C. A homogenization temperature of CO_2 (T_h CO_2) was recorded between +19.9 and +27.4 °C (into the liquid phase) and between +24.0 and +24.3 °C (into the vapour phase). For Raman microspectrometry studies, some aqueous carbonic inclusions present in sample ASM020 (G0) were selected. CO_2 and N_2 were the only gaseous species detected. CO_2 was the dominant species in the volatile phase ranging from 76.35 to 89.56 mol % and N_2 contents ranged from 10.44 to 23.65 mol %.

https://doi.org/10.1017/S0016756814000569 Published online by Cambridge University Press

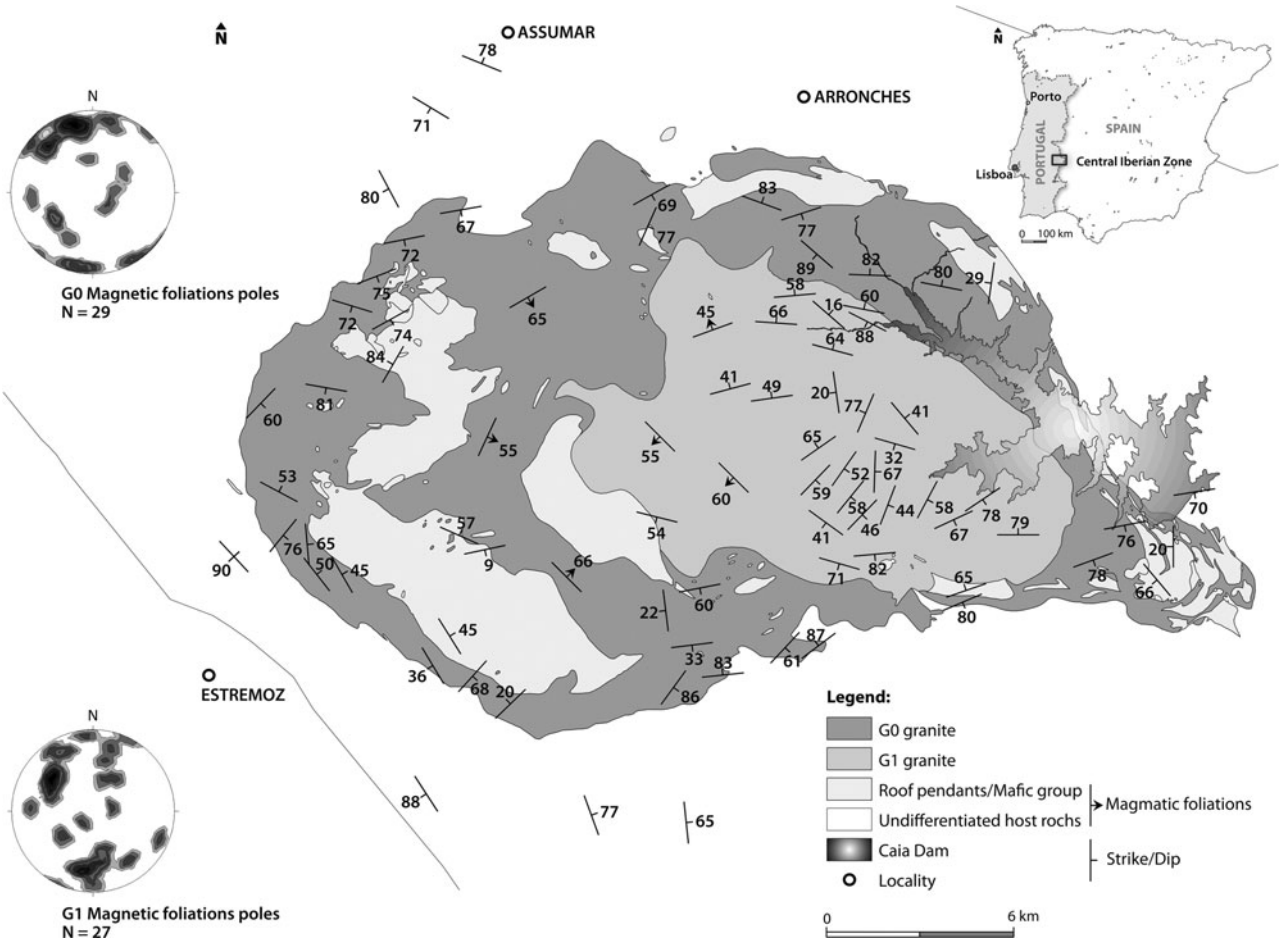

Figure 8. Map of the magnetic foliations with orientation stereonets for the magnetic foliations poles (K_3) for G0-type and G1-type (Schmidt, lower hemisphere projection, 1–5 % area contours).

5.b. Aqueous fluids (H_2O+NaCl)

This type (LW_1) is the most common in all samples. The data indicate a predominance of low- to medium-salinity aqueous inclusions in both granites of the SEPC, ranging in size from 4 to 25 μm in longest dimension. The ice melting temperature in G0 ($T_{m,ice}$) was observed as between –8.0 and –0.9 °C (LW_1), corresponding to low and medium salinity ranging from 0.18 to 11.70 wt % eq. NaCl. In G1, $T_{m,ice}$ ranges between –8.0 and –2.6 °C (LW_1). The global homogenization observed was always into liquid phase with the temperatures T_h observed in the range +134 to +270 ºC (G0-type) and +224 to +310 ºC (G1-type).

5.c. Aqueous fluids (NaCl–CaCl)

This type of inclusion (LW_2) was recorded only in one sample of G0-type. They have moderate to high salinities (between 14.3 and 21.0 wt % eq. NaCl + CaCl) with first ice melting temperatures of <–50 °C. These correspond to eutectic temperatures, which might indicate the presence of Ca chloride.

6. Interpretation and discussion

6.a. Significance of magnetic susceptibility and isothermal remanent magnetization values

The SIRM analyses together with magnetic susceptibility values (Fig. 14) show that two distinct groups of magnetic behaviour are evident: G0 and M-group with higher SIRM and K_m values; and G1 with lower values. In G0, isothermal remanent magnetization acquisition curves show that, at some sites, the main carrier of the remanence is a ferrimagnetic fraction (low magnetite or Ti-magnetite). These data are also confirmed by the K_m values found; at 29 sites, 10 have $K_m > 10^{-3}$ SI. In G1 however, $K_m < 10^{-4}$ SI indicates a paramagnetic behaviour due to ferromagnesian minerals (e.g. biotite) and iron oxides (e.g. ilmenite). This is also shown on the isothermal remanent magnetization curves, which indicates a dominant paramagnetic fraction. The mean ratio of the isothermal remanent magnetization at 300 mT (IRM_{300}) to saturation isothermal remanent magnetization (SIRM), referred to as S_{300}, provides a comparative measure of the amounts of high-coercivity and low-coercivity remanence (Bloemendal, Lamb & King, 1988). S_{300} is 0.960 for the 10 sites of G0, confirming the presence of a ferrimagnetic fraction.

https://doi.org/10.1017/S0016756814000569 Published online by Cambridge University Press

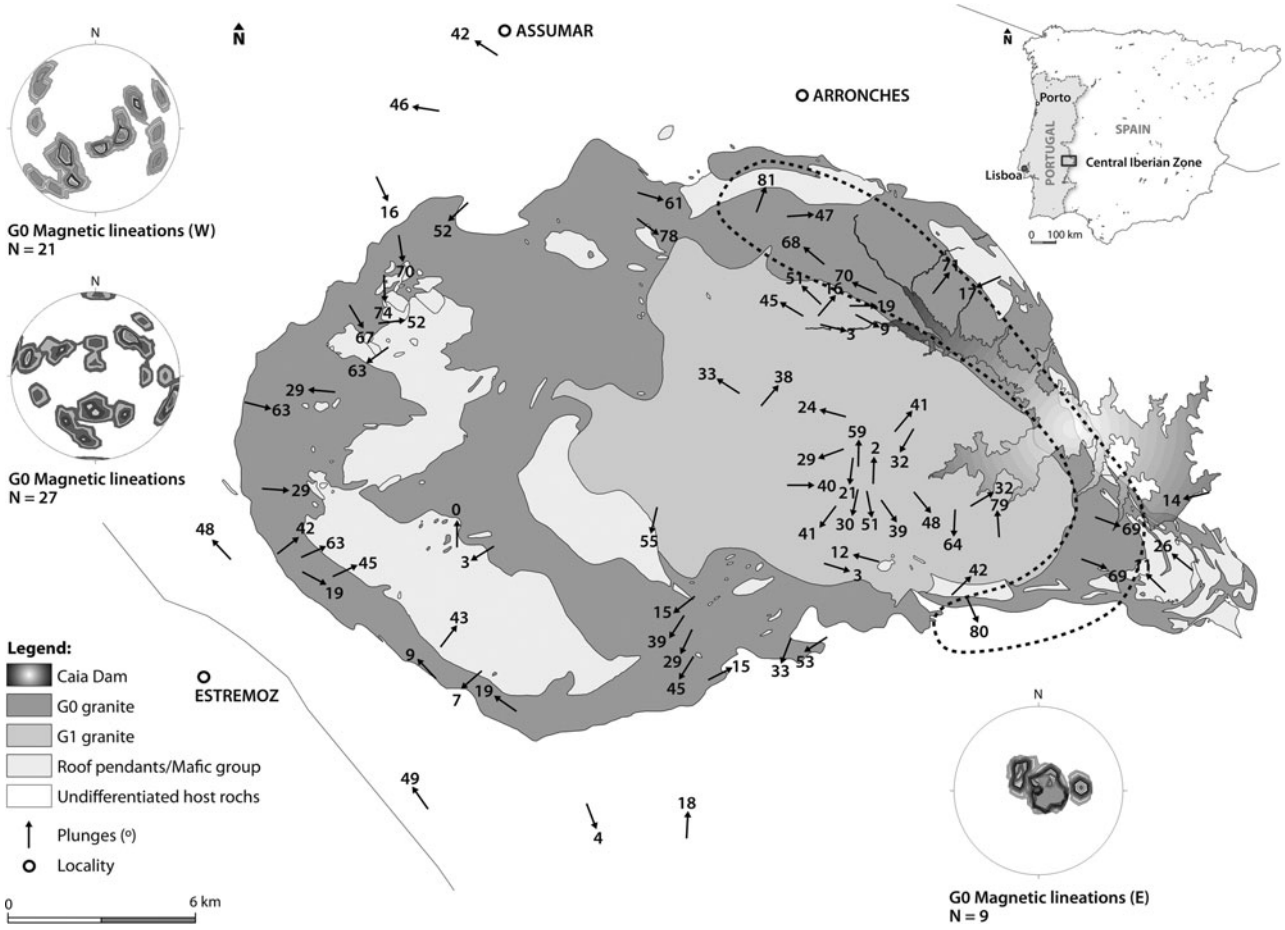

Figure 9. Map of the magnetic lineations with orientation stereonets for the magnetic lineations (K_1) for G0-type (sector E and W) and G1-type (Schmidt, lower hemisphere projection, 1–5 % area contours). Magmatic foliations are defined by preferred alignment of biotite and feldspar crystals.

In basic rocks from the M-group, the values of K_m are typical of those usually found in gabbros and granodiorites. It is due to the high content of ferromagnesian minerals and probably also to the presence of magnetite, as indicated by the shape of the isothermal remanent magnetization curves.

In host rocks and roof pendant rocks, K_m and SIRM values demonstrate a wide range. The different shapes of the isothermal remanent magnetization curves emphasize the variety of magnetic structures present in the different lithologies.

The mean values of the ratio of saturation isothermal remanent magnetization to magnetic susceptibility (SIRM/K_m) are similar for G0 and M, but not G1. According to several authors (e.g. Thompson & Oldfield, 1986; Sandgren & Thompson, 1990), when ferrimagnetic structures are present SIRM/K_m can be used as an indicator of magnetic mineral grain size. Sandgren and Thompson (1990) indicated that a value of 6.4 kA m^{-1} corresponds to a magnetite grain size of 8 μm. Based on these authors, the mean value of the ratio of SIRM to magnetic susceptibility of 7.12 kA m^{-1} obtained in G0 could indicate a similar magnetite grain size.

These data are confirmed by the thermomagnetic experiments, which indicate the presence of magnetite in G0 and the paramagnetic behaviour of G1. The magnetic behaviours of G0 and G1 suggest different redox conditions in the magma genesis; according to Ishihara (1977), G0 may be considered as a magnetite-type granite while G1 is an ilmenite-type granite. The magnetite-series granites are scarce in Portuguese Variscan granites. Furthermore, the existence of two different granite series in the same pluton is very uncommon. Magnetite and ilmenite-series granites are primarily governed by the prevailing fO_2 (fugacity of oxygen; Ishihara, 1977). Carmichael (1991) established that the redox states of silicic and basic magmas are inherited from their respective source regions. Nevertheless, some granites may acquire their oxidation or reduction state due to specific physico-chemical conditions. The interaction processes of mafic and felsic magma mixing and mingling, which occur in an open system, can also play an important role in increasing the oxidizing conditions of magma chambers (Kumar, 2010).

Menéndez *et al.* (2006) proposed a partial melting of intermediate igneous and metasedimentary lithologies in the low–middle crust as the source of G0 and G1 types (although petrogenetically independent) and a mantle source for the M-group.

We consider that the formation of magnetite G0-type required oxidized conditions related to the interaction of the mafic rocks of M-group with felsic magma,

https://doi.org/10.1017/S0016756814000569 Published online by Cambridge University Press

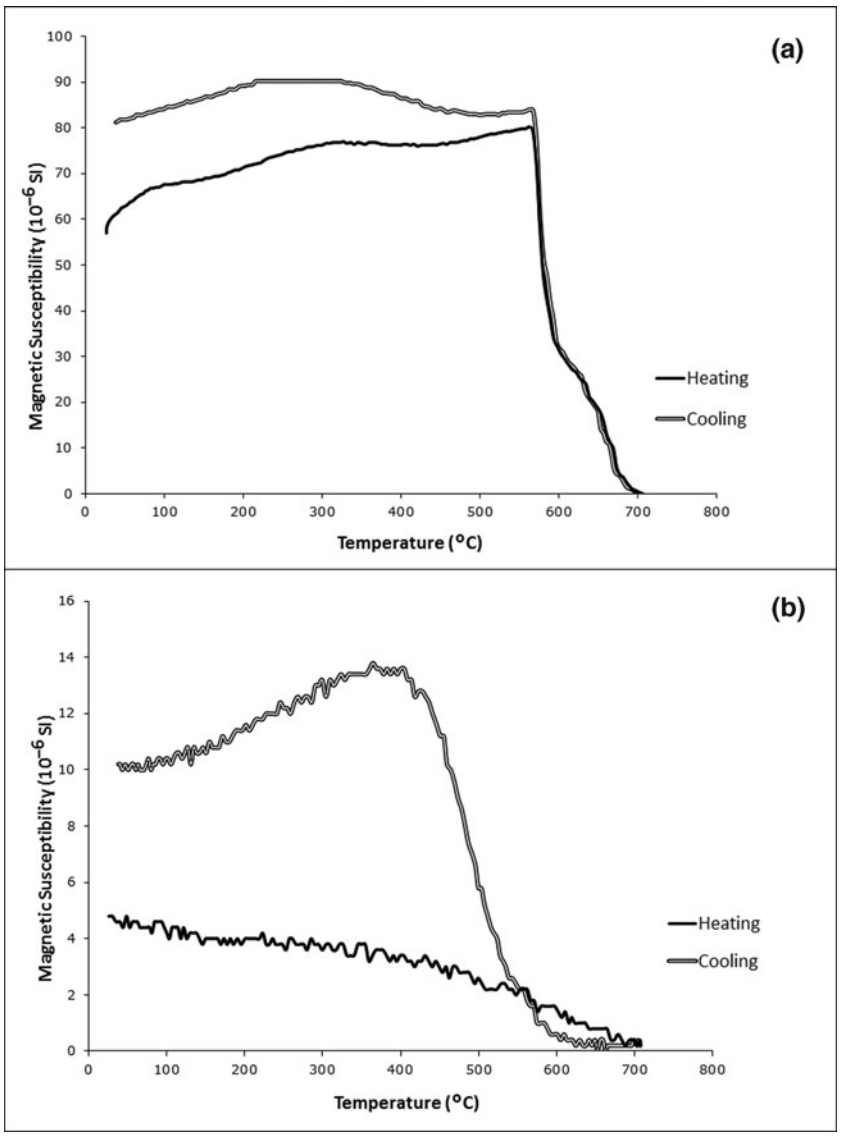

Figure 10. Normalized magnetic susceptibility curves for continuously increasing (and decreasing) temperatures for (a) G0 (ASM76), showing dominantly ferromagnetic behaviour with magnetic susceptibility drop at 580 °C; and (b) G1 (Af57), showing dominantly paramagnetic behaviour with a decrease in magnetic susceptibility with increasing temperature.

whereas the ilmenite G1-type could have been formed by assimilation of organic carbon from the accreted sediments in the lower–middle crust (e.g. Ishihara & Matsuhisa, 1999).

6.b. Magnetic fabric

The degree of magnetic anisotropy increases towards the margin. Magnetic anisotropy is higher in G0 compared to G1 and P of >11 % is found in the sites with magnetite. We assume that the increasing magnetic anisotropy towards the margin is related to the magmatic strain increase; even in the sites of G0 that do not have magnetite, the anisotropy is always higher that in G1. This assumption is confirmed by microscope observations that show signs of a post-magmatic deformation in G0 rather than in G1. The degree of oblateness does not increase towards the margin; instead, the strongest oblate ellipsoids are in the central facies and the prolate ellipsoids are mainly present in the western part of G0. The oblate ellipsoids present at most G0 and G1 sites are mainly due to the magnetocrystalline anisotropy of biotite, but can also be related to the oblate shape anisotropy of magnetite grains. The prolate ellipsoids found in the western part form steep contacts with the wall rocks.

The magnetic foliations are steep in both granites and ENE–WSW-striking, defining a dome in G1 but dipping inwards in G0 and outwards in G1. Magnetic lineations exhibit three distinct orientations: subvertical in the east sector of G0; plunging moderated at variable trends in G1; and to the SW in the west sector of G0.

6.c. Emplacement model

To understand granite ascent and emplacement processes it is important to consider the granites of SEPC and the crustal discontinuities that surround them simultaneously.

https://doi.org/10.1017/S0016756814000569 Published online by Cambridge University Press

Table 2. Saturation isothermal remanent magnetization (SIRM), isothermal remanent magnetization at 300 mT (IRM_{300}), ratio of SIRM to magnetic susceptibility (SIRM/K) and ratio of IRM_{300} to SIRM in representative samples of the SEPC.

Sampling sites	Lithology	SIRM (A m^{-1})	IRM_{300} (A m^{-1})	SIRM/K (kA m^{-1})	$S_{300} = IRM_{300}/SIRM$
ASM 005 F2	M-Group	4.135	4.036	4.957	0.976
ASM 005 D2	M-Group	5.657	5.549	6.783	0.981
ASM 010 C	M-Group	0.580	0.339	1.088	0.585
ASM 015 B1	M-Group	2.172	2.137	3.267	0.984
ASM 070 B2	M-Group	0.623	0.599	1.028	0.960
Af3 Maf B2	Roof pendants	0.062	0.029	0.137	0.471
ASM J58 B1	Roof pendants	0.875	0.640	3.008	0.731
ASM 026 B1	Roof pendants	0.007	0.007	0.010	0.979
ASM 027 F	Host rocks	0.096	0.089	0.262	0.932
ASM JD1 B1	Host rocks	0.011	0.010	0.372	0.869
Af6.0Enc C1	Host rocks	20.776	14.761	43.758	0.710
ASM 001 B1	G0	1.249	0.670	13.189	0.536
ASM 002 B1	G0	5.874	5.376	4.484	0.915
ASM 003 B1	G0	6.158	5.186	11.751	0.842
ASM 004 D1	G0	3.601	3.478	2.131	0.966
ASM 016 B1	G0	0.789	0.466	6.685	0.590
ASM 017 A1	G0	9.414	9.107	5.958	0.967
ASM 017 B1	G0	11.986	11.532	6.514	0.962
ASM 020 A2	G0	1.762	1.363	7.974	0.774
ASM 020 B1	G0	2.530	2.100	12.975	0.830
ASM 069 C1	G0	2.246	2.253	1.075	1.003
ASM 012 B2	G0	28.558	28.311	6.849	0.991
ASM 002 E1	G0	7.051	6.453	6.779	0.915
ASM 017B2	G0	8.820	8.402	5.573	0.953
Af 1.0 C1	G0	4.372	3.788	7.243	0.867
Af 2.0 C2	G0	3.347	2.091	5.212	0.625
Af 8.0 C	G0	51.762	50.067	9.520	0.967
ASM 006 A2	G1	0.027	0.027	0.287	0.996
ASM 006 C1	G1	0.005	0.004	0.054	0.768
ASM 009 A2	G1	0.026	0.024	0.279	0.944
ASM 022 B1	G1	0.010	0.008	0.098	0.886
ASM 029 A2	G1	0.021	0.017	0.255	0.833
ASM 009 E1	G1	0.052	0.049	0.563	0.939
ASM 009B2	G1	0.017	0.015	0.072	0.902
ASM 007 A2	G1	0.040	0.031	0.364	0.782
ASM 008 A2	G1	0.022	0.019	0.181	0.876
ASM 011 A2	G1	0.026	0.022	0.238	0.860
ASM 021 A2	G1	0.031	0.028	0.221	0.911
ASM 023C1	G1	0.033	0.009	0.594	0.265
ASM 024 B1	G1	0.043	0.028	0.672	0.656

The northern limit of the Ossa Morena Zone is characterized by a transpressive–transtensive tectonic regime (Harland, 1971) with strain concentration along subvertical sinistral shear zones, oriented NW–SE (e.g. Araújo *et al*. 2013) in the same way as the Coimbra–Córdoba Shear Zone. These NW–SE shear zones, with continuity exceeding hundreds of kilometres, reflect deeply rooted discontinuities in the crust (e.g. Pereira *et al.* 2013). The occurrence of NE–SW and ENE–WSW conjugate fault systems perpendicular to the regional structures is related to the final brittle stages of the Variscan Orogeny. The late Variscan fracturing is represented by the development of NNW–SSE (right) and NE–SW (left) conjugate pairs, indicating a north–south main compression (Ribeiro *et al.* 1979). Previous right-lateral NE–SW faults, such as the Messejana fault, display left-lateral behaviour at this stage.

The kinematic mechanism described operated from the earliest stages of ductile deformation (at 370 Ma) to the last phase of ductile regional deformation (at 306 Ma), until the final stages of brittle deformation (Ribeiro *et al.* 2007). As a working hypothesis we suggest that these NW–SE structures are possible escape zones, inducing local decompression and the consequent initiation of partial melting that, primarily, facilitated granite ascent.

We propose that the ascent of the magma took place in the eastern part of the body, attested by the subvertical G0 magnetic lineations and 2D modelling. The intersection between the Assumar strike-slip fault (associated with the Coimbra–Córdoba Shear Zone) and Messejana fault (Fig. 1) promoted the structural conditions for magma ascent and emplacement. The magma emplacement was controlled by the existing ENE–WSW planar anisotropies that allowed the expansion of the granitic complex and are recorded by the magnetic foliations in the two granitic types. The gravimetric data together with the magnetic fabric indicate that the G0-type is a tabular flat-floored massif, with magnetic foliations dipping towards the interior of the pluton. For the G1-type the combined data show a rooted dome-like structure with outwards dipping magnetic foliations. The feeder zone of the pluton is located towards the eastern part of the pluton, confirming the role of the Assumar and Messejana faults in the process of emplacement.

https://doi.org/10.1017/S0016756814000569 Published online by Cambridge University Press

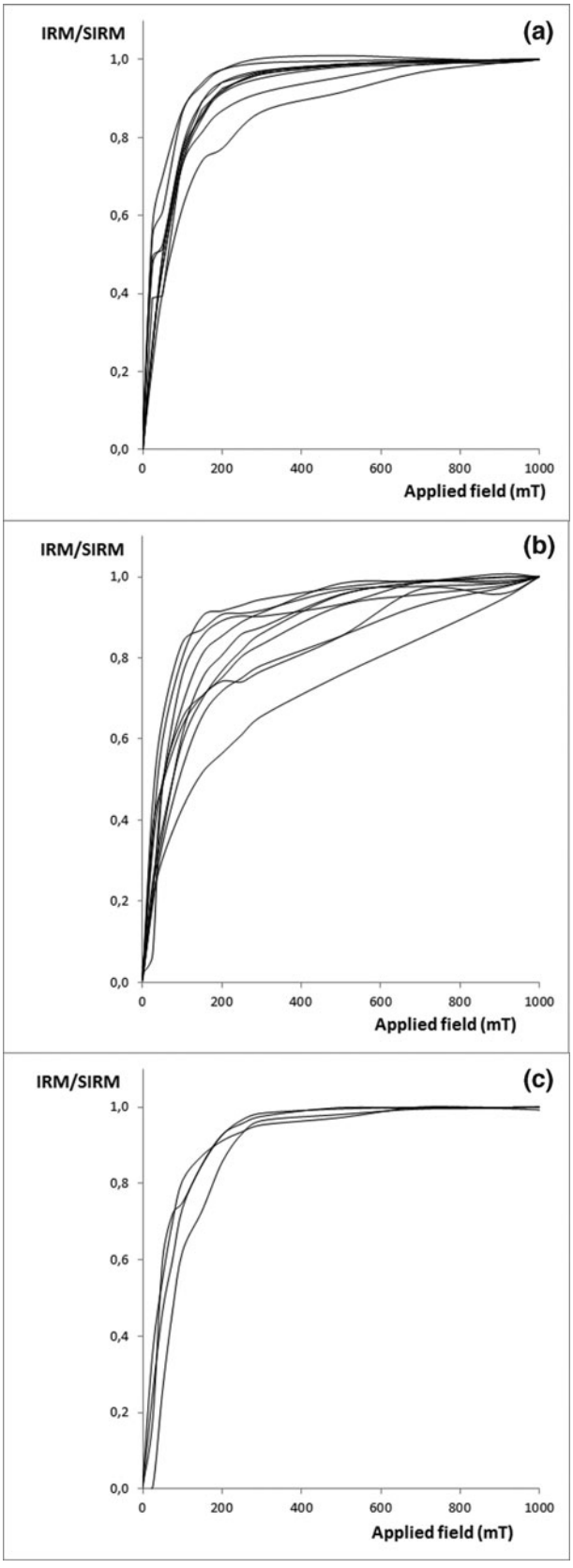

Figure 11. IRM normalized (IRM/SIRM) acquisition curves for the representative samples from (a) G0, (b) G1 and (c) M-group.

Granitic bodies such as Fronteira, Ervedal and Vimieiro–Pavia (Gonçalves, 1971; Palácios, 1976) define an east–west magmatic set with an alignment consistent with this interpretation.

It is also significant that thermal effects in the host rocks caused by the intrusion of the SEPC are restricted to the roof pendants cropping out in the western part of the SEPC. The lack of thermal overprint on the wall rocks highlights the small thickness of G0-type, also corroborated by the 2D modelling and by the magnetic lineations that plunge moderately.

The emplacement of the two granites was passive and almost synchronous, as shown by their gradational contacts found in the field. Although the magnetic fabric suggests emplacement of the G0-type was first, utilizing subvertical ENE–WSW crustal fractures, the magma flow was mainly SW directed as magnetic lineations show. The G0 emplacement was closely followed by the G1, pushing the G0 laterally which become more anisotropic towards the margin. The G1-type became flattened, acquiring a dome-like structure. This chronological sequence was also proposed by Menéndez *et al*. (2006) based on geochemical data. The two granites of SEPC formed a nested pluton.

Stoping is a widely accepted emplacement (e.g. Marsh, 1982; Glazner & Bartley, 2006) mechanism, and its applicability to SEPC should be discussed. Stoping occurs when blocks of wall rock are transferred downwards through a pluton, and has been widely used to explain discordant pluton contacts. However, the common signatures of stoping are sharp discordant contacts between plutons and wall rocks and a lack of ductile deformation of the wall rocks (e.g. Glazner & Bartley, 2006; Žák, Holub & Kachlík, 2006). The northeast wall rocks of SEPC are deflected by the intrusion which means they were still ductile during the G0 emplacement, ruling out stoping as emplacement mechanism. The expansion of G0 was accompanied by a downwards return of magmatic flow deflecting the wall rocks at the northeast, a process observed in other plutons (e.g. Paterson & Vernon, 1995; Paterson, Fowler & Miller, 1996; Sylvester, 1998).

The Rb–Sr age of 290 Ma (Pinto, 1984) of the SEPC and the lack of solid-state microstructures imply that the emplacement of the SEPC could be considered as late- to post-tectonic.

After emplacement, the SEPC recorded increments of the regional tectonic strain as documented by fluid inclusion planes in quartz. All the fluid inclusion planes are post-magmatic; no relationship with the magnetic fabric could therefore be established. Nevertheless, the fluid inclusion planes (Fig. 13) indicate that the stress field was different in the two granites. The fluid inclusion planes in G0-type, which are parallel to the regional structures, suggest that the stress field during the cooling process was rotated locally to the NW–SE direction. The predominant direction of the fluid inclusion planes of G1-type, NNE–SSW to NE–SW, is compatible with the stress field (NE–SW to N–S maximum compressive stress) prevailing in the final stages of the Variscan Orogeny during the cooling of this granite. The magnetic fabric of the SEPC does not reveal any structural pattern related to the near-solidus thermal contraction of igneous mass or to the

https://doi.org/10.1017/S0016756814000569 Published online by Cambridge University Press

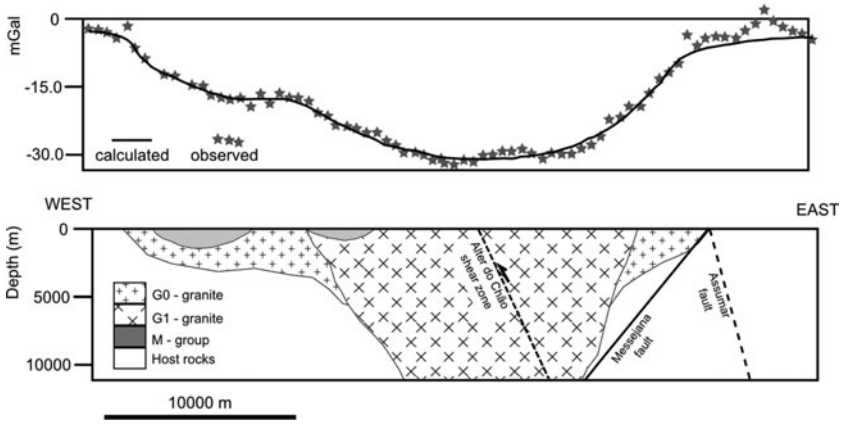

Figure 12. 2D Gravity modelling through the SEPC along E–W-oriented cross-sections.

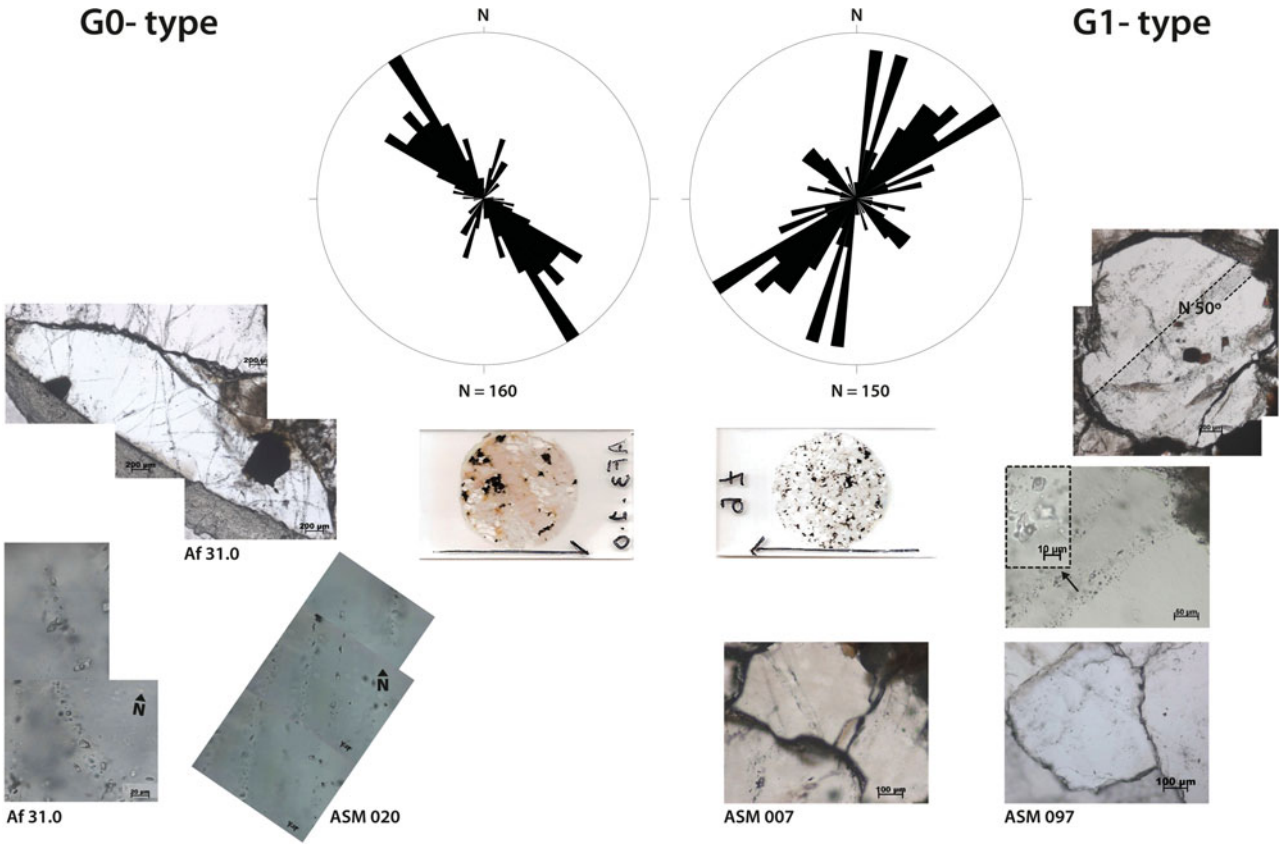

Figure 13. (Colour online) Rose diagrams indicating the preferential orientation of the fluid inclusions planes. Example of oriented double-polished wafers and some studied fluid inclusions representative of the predominant orientations of quartz.

fluid inclusion planes directions, as was found in other intrusions (Gil-Imaz *et al*. 2006).

The aqueous carbonic fluid inclusions found in the G0-type suggests that there was an interaction between the carbonate host rocks and the G0-type. The high-salinity fluids found in the G0-type may be related to the deep circulation of fluids linked to the neighbourhood of the Messejana fault. The aqueous fluids record the hydrothermal events that took place during the post-magmatic processes.

The kinematical features found in this work therefore seem to describe the continuous sequence of events which occurred during the emplacement and the cooling of the granitic magmas over a short time frame.

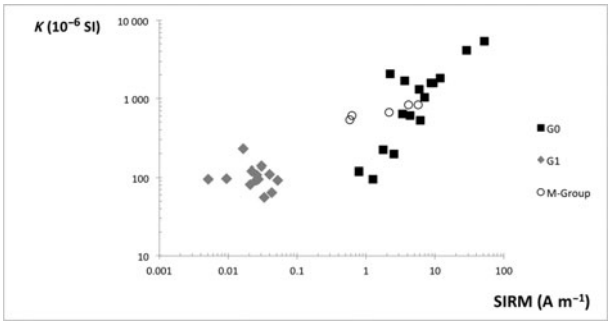

Figure 14. Plot of the relation between SIRM and magnetic susceptibility *K* for representative samples of G0, G1 and M-group.

https://doi.org/10.1017/S0016756814000569 Published online by Cambridge University Press

7. Conclusions

- The SEPC is a nested intrusion composed of two granites, G0 and G1, with different magnetic behaviours, suggesting different redox conditions in the magma genesis. G0 may be considered a magnetite-type granite, while G1 is an ilmenite-type granite. The formation of G0-type required oxidized conditions related to the interaction of the mafic rocks of the M-group with felsic magma.
- The feeder zone of the pluton is located in the eastern part of the pluton, confirming the role of the Assumar and Messejana faults in the process of ascent and emplacement.
- The magma emplacement was controlled by the existing ENE–WSW planar anisotropies related to the final brittle stages of the Variscan Orogeny, which allowed the expansion of the granitic complex. These are recorded by the magnetic foliations in the two granitic types.
- Both gravity modelling and magnetic fabric data indicate that the G0-type is a tabular, flat-floored massif with magnetic foliations dipping towards the interior of the pluton. G1-type forms a rooted dome-like structure with outwards dipping magnetic foliations.
- The emplacement of the two granites was passive and almost synchronous, as shown by their gradational contacts found in the field. However, the magnetic fabric suggests the G0-type was emplaced first, closely followed by the G1-type. The G1-type pushed the G0 laterally, which become more anisotropic towards the margin. The G1-type became flattened, acquiring a dome-like structure. The two granites of the SEPC formed a nested pluton.
- After emplacement, the SEPC recorded increments of the late Variscan stress field, documented by fluid inclusion planes in quartz.
- The Rb–Sr ages of 290 Ma and the lack of solid-state microstructures mean that the emplacement of the SEPC can be considered as late- to post-tectonic.

Acknowledgements. This work was financially supported by PTDC/CTE-GIX/099447/2008 (FCT-Portugal, COMPETE/FEDER). The authors thank Philippe Olivier for the thermomagnetic measurements carried out in Toulouse. We thank Jirí Zak and an anonymous referee for their helpful comments.

Supplementary material

To view supplementary material for this article, please visit http://dx.doi.org/10.1017/S0016756814000569

References

ARAÚJO, A., PIÇARRA ALMEIDA, J., BORREGO, J., PEDRO, J. & OLIVEIRA, J. T. 2013. As regiões centro e sul da Zona de Ossa Morena. In *Geologia de Portugal, Volume I, Geologia Pré-mesozóica de Portugal* (eds R. Dias, A. Araújo, P. Terrinha & J. C. Kullerberg), pp. 509–49. Lisboa: Escolar Editora.

BAKKER, R. J. 2003. Package FLUIDS 1. Computer programs for analysis of fluid inclusion data and for modeling bulk fluid properties. *Chemical Geology* **194**, 3–23.

BLOEMENDAL, J., LAMB, J. B. & KING, J. 1988. Paleoenvironmental implications of rock-magnetic properties of late quaternary sediment cores from the eastern equatorial Atlantic. *Paleoceanography* **3**(1), 61–87.

BODNAR, R. J. 1993. Revised equation and table for determining the freezing point depression of H_2O-NaCl solutions. *Geochimica et Cosmochimica Acta* **57**, 683–4.

BORRADAILE, G. J. 1988. Magnetic susceptibility, petrofabrics and strain. *Tectonophysics* **156**, 1–20.

BORRADAILE, G. J. & HENRY, B. 1997. Tectonic applications of magnetic susceptibility and its anisotropy. *Earth Science Reviews* **42**, 49–93.

BOUCHEZ, J. L. 1997. Granite is never isotropic: an introduction to AMS studies of granitic rocks. In *Granite: From Melt to Emplacement Fabrics* (eds J. L. Bouchez, D. H. W. Hutton & W. E. Stephens), pp. 95–112. Dordrecht: Kluwer Academic Publishers.

BRANTLEY, S. L. 1992. The effect of fluid chemistry on microcracks life-times. *Earth and Planetary Science Letters* **113**, 145–56.

CARMICHAEL, I. S. E. 1991. The redox states of basic and silicic magmas: a reflection of their source regions? *Contributions to Mineralogy and Petrology* **106**, 129–41.

COLLINSON, D. W. 1983. *Methods in Rock Magnetism and Paleomagnetism: Techniques and Instrumentation*. London: Chapman and Hall.

CRUZ, C., RIBEIRO, M. A. & SANT'OVAIA, H. 2013. Thermal effects of the Santa Eulália Plutonic Complex (Southern Portugal) on the metaigneous and metasedimentary host rocks. In *IX Congreso Ibérico e IX Congreso Nacional de Geoquímica. Session de póster*, pp. 31–33. Soria, September 2013.

DÓRIA, A., RIBEIRO, M. A., SANT'OVAIA, H. & FERNANDES, F. 2011. Host rocks of Santa Eulalia Plutonic Complex (Southern Portugal): A preliminary study. *Mineralogical Magazine* **75**(3), 774.

DÓRIA, A., SANT'OVAIA, H., RIBEIRO, M. A. & ALVES, M. 2009. Fluid inclusions planes and anisotropy of magnetic susceptibility studies in Porto granite massif (northern Portugal). *Geochimica et Cosmochimica Acta Goldschmidt Conference Abstracts* **73**(13, S1), A300.

FONSECA, P. 1995. *Estudo da Sutura Varisca no SW Ibérico nas regiões de Serpa-Beja-Torrão e Alvito-Viana do Alentejo*. Ph.D. thesis, Lisboa University, Lisboa. Published thesis.

FONSECA, P., MUNHÁ, J., PEDRO, J., ROSAS, F., MOITA, P., ARAÚJO, A. & LEAL, N. 1999. Variscan ophiolites and high-pressure metamorphism in Southern Iberia. *Ofioliti* **24**(2), 259–68.

FROST, B. R., BARNES, C. G., COLLINS, W. J., ARCULUS, R. J., ELLIS, D. J. & FROST, C. D. 2001. A geochemical classification for granitic rocks. *Journal of Petrology* **42**, 2033–48.

FROST, C. D. & FROST, B. R. 2011. On Ferroan (A-type) granitoids: their compositional variability and modes of origin. *Journal of Petrology* **52**, 39–53.

GIL-IMAZ, A., POCOVÍ, A., LAGO, M., GALÉ, C., ARRANZ, E., RILLO, C. & GUERRERO, E. 2006. Magma flow and thermal contraction fabric in tabular intrusions inferred from AMS analysis. A case study in a late-Variscan folded sill of the Albarracín Massif (southeastern Iberian Chain, Spain). *Journal of Structural Geology*, **28**, 641–53.

GLAZNER, A. F. & BARTLEY, J. M. 2006. Is stoping a volumetrically significant pluton emplacement process? *GSA Bulletin* **118**, 1185–95.

GONÇALVES, F. 1971. Subsídios para o conhecimento geológico do Nordeste Alentejano. *Memórias Serviços Geológicos de Portugal* **18**, 1–62.

GRAHAM, J. W. 1954. Magnetic susceptibility anisotropy, an unexploited petrofabric element. *Geological Society of America Bulletin* **65**, 1257–8.

HARLAND, W. B. 1971. Tectonic transpression in Caledonian Spitzbergen. *Geological Magazine* **108**, 27–42.

HELLER, F. 1973. Magnetic anisotropy of granitic rocks of the Bergell Massif (Switzerland). *Earth Planetary and Science Letters* **20**, 180–8.

HROUDA, F. 1982. Magnetic anisotropy of rocks and its application in geology and geophysics. *Geophysical Surveys* **5**, 37–82.

ISHIHARA, S. 1977. The magnetite-series and ilmenite-series granitic rocks. *Mining Geology* **27**, 292–305.

ISHIHARA, S. & MATSUHISA, Y. 1999. Oxygen isotope constraints on the genesis of the Miocene Outer Zone Granitoids in Japan. *Lithos* **46**, 523–34.

JELINEK, V. 1981. Characterization of the magnetic fabric of rocks. *Tectonophysics* **79**, 63–7.

JESUS, A., MUNHÁ, J., MATEUS, A., TASSINARI, C. & NUTMAN, A. 2007. The Beja Layered Gabbroic Sequence (Ossa-Morena Zone, Southern Portugal): geochronology and geodynamic implications. *Geodinamica Acta* **20**(3), 139–57.

KUMAR, S. 2010. Magnetite and ilmenite series granitoids of Ladakh batholith, Northwest Indian Himalaya: implications on redox conditions of subduction zone magmatism. *Current Science* **99**(9), 1260–4.

LESPINASSE, M. 1999. Are fluid inclusion planes useful in structural geology? *Journal of Structural Geology* **21**, 1237–43.

LESPINASSE, M. & CATHELINEAU, M. 1995. Paleostress magnitudes determination by using fault slip and fluid inclusions planes data. *Journal of Geophysical Research* **100**, 3895–904.

LESPINASSE, M. & PECHER, A. 1986. Microfracturing and regional stress field: a study of preferred orientations of fluid inclusion planes in a granite from the Massif Central, France. *Journal of Structural Geology* **8**, 169–80.

LIMA, S. 2013. *Magmatic evolution of the Pavia pluton (Ossa-Morena Zone): Geochemical and Geochronological constraints*. Ph.D. thesis, Faculdade de Ciências e Tecnologia da Universidade de Coimbra. Published thesis.

LOPES, L., CARRILHO, J., SANT'OVAIA, H., NOGUEIRA, P. & RIBEIRO, M. A. 2013. Petrology, geochemistry and structural control of a late variscan ring pluton: the Santa Eulalia plutonic complex (Alentejo, Portugal). In *Proceedings of GSA Annual Meeting*, Denver, October 2013.

LOPES, J. M. C., LOPES, J. L. & LISBOA, J. V. 1997. Caracterização petrográfica e estrutural dos granitos róseos do Complexo Plutónico de Monforte – Santa Eulália (NE-Alentejo, Portugal). *Estudos, Notas e Trabalhos, Instituto Geológico e Mineiro* **39**, 141–57.

LOPES, J. M. C., MUNHÁ, J., WU, C. T. & OLIVEIRA, V. M. J. 1998. O Complexo Plutónico de Monforte-Santa Eulália (Alentejo-NE, Portugal Central): caracterização geoquímica e considerações petrogenéticas. *Comunicações do Instituto Geológico e Mineiro* **83**, 127–42.

MARSH, B. D. 1982. On the mechanics of igneous diapirism, stoping, and zone melting. *American Journal of Science* **282**, 808–55.

MARTINS, H. C. B., SANT'OVAIA, H., ABREU, J., OLIVEIRA, M. & NORONHA, F. 2011. Emplacement of the Lavadores granite (NW Portugal): U/Pb and AMS results. *Comptes Rendus Geoscience* **343**, 387–96.

MARTINS, H. C. B., SANT'OVAIA, H. & NORONHA, F. 2009. Genesis and emplacement of felsic Hercynian plutons within a deep crustal lineation, the Penacova-Régua-Verín fault: an integrated geophysics and geochemical study (NW Iberian Peninsula). *Lithos* **111**, 142–55.

MARTINS, H. C. B., SANT'OVAIA, H. & NORONHA, F. 2013. Late-Variscan emplacement and genesis of the Vieira do Minho composite pluton, Central Iberian Zone: constraints from U-Pb zircon geochronology, AMS data and Sr-Nd-O isotope geochemistry. *Lithos* **162–163**, 221–35.

MATTE, P. 2001. The Variscan collage and orogeny (480–290 Ma) and the tectonic definition of the Armorica microplate: a review. *Terra Nova* **13**, 122–8.

MENÉNDEZ, L. G., AZOR, A., PEREIRA, M. D. & ACOSTA, A. 2006. Petrogénesis de plutón de Santa Eulália (Alto Alentejo, Portugal). *Revista de la Sociedad Geológica de España* **19**(1–2), 69–86.

MOITA, P., MUNHÁ, J., FONSECA, P., PEDRO, J., TASSINARI, C., ARAÚJO, A. & PALÁCIOS, T. 2005. Phase equilibrium and geochronology of Ossa-Morena eclogites. In *XIV Semana de Geoquímica* and *VIII Congresso de geoquímica dos Países de Língua Portuguesa*, Universidade de Aveiro, Portugal, **2**, 471–4.

MOITA, P., SANTOS, J. F. & PEREIRA, M. F. 2009. Layered granitoids: Interaction between continental crust recycling processes and mantle-derived magmatism. Examples from the Évora Massif (Ossa-Morena Zone, southwest Iberia, Portugal). *Lithos* **111**, 125–41.

MUNHÁ, J., OLIVEIRA, J. T., RIBEIRO, A., OLIVEIRA, V., QUESADA, C. & KERRICH, R. 1986. Beja-Acebuches ophiolite characterization and geodynamic significance. *Maleo* **2**(13), 31.

OLIVEIRA, J. T., OLIVEIRA, V. & PIÇARRA, J. M. 1991. Traços gerais da evolução tectonp-estratigráfica da Zona Ossa Morena. *Comunicações dos Serviços Geológicos de Portugal* **77**, 3–26.

PALÁCIOS, T. 1976. Contribuição para o conhecimento petrográfico do maciço granítico de Fronteira e comparação com os de Ervedal e Santa Eulália (Nordeste alentejano). *Comunicações dos Serviços Geológicos de Portugal* **LX**, 239–60.

PATERSON, S. R., FOWLER, T. K., JR. & MILLER, R. B. 1996. Pluton emplacement in arcs: A crustal-scale exchange process. *Transactions of the Royal Society of Edinburgh: Earth Sciences* **87**, 115–23.

PATERSON, S. & VERNON, R. H. 1995. Bursting the bubble of ballooning plutons: a return to nested diapirs emplaced by multiple processes. *Geological Society of America Bulletin* **l07**, 1356–80.

PEREIRA, M. F., SILVA, J. B., SOLÁ, A. R. & CHICHORRO, M. 2013. Nordeste Alentejano. In *Geologia de Portugal, Volume I, Geologia Pré-mesozóica de Portugal* (eds R. Dias, A. Araújo, P. Terrinha & J. C. Kullerberg), pp. 493–508. Lisboa: Escolar Editora.

PEREIRA, M. F., SILVA, J. B., SOLÁ, A. R., CHICHORRO, M., MOITA, P., SANTOS, J. F., APRAIZ, A. & RIBEIRO, C. 2007. Crustal growth and deformation process in the northern Gondwana margin: Constraints from the Évora Massif (Ossa-Morena Zone, southwest Iberia, Portugal). In

The Evolution of the Rheic Ocean: From Avalonian–Cadomian Active Margin to Alleghenian–Variscan Collision (eds U. Linnemann, R. D. Nance, P. Kraft & G. Zulauf), pp. 333–58. Geological Society of America, Special Paper no. 423.

PIN, C., FONSECA, P. E., PAQUETTE, J. L., CASTRO, P. & MATTE, P. 2008. The ca. 350 Ma Beja Igneous Complex: a record of transcurrent slab-break off in the Southern Iberia Variscan Belt? *Tectonophysics* **461**, 365–77.

PINTO, M. S. 1984. Granitóides Caledónicos e Hercínicos na Zona Ossa Morena (Portugal). *Memórias e Notícias, Publicações do Museu e Laboratório Mineralógico e Geológico da Universidade de Coimbra (Portugal)* **97**, 81–94.

POTY, B., LEROY, J. & JACHIMOWICZ, L. 1976. Un nouvel appareil pour la mesure des températures sous le microscope, l'installation de microthermométrie Chaixmeca. *Bulletin de la Société Française de Minéralogie et de Cristallographie* **99**, 182–6.

PRIETO, A. C., GUEDES, A., DÓRIA, A., NORONHA, F. & JIMÉNEZ, J. 2012. Quantitative determination of gaseous phase compositions in fluid inclusions by Raman microspectrometry. *Spectroscopy Letters* **45**, 156–60.

QUESADA, C. 2006. The Ossa-Morena Zone of the Iberian Massif: a tectonostratigraphic approach to its evolution. *Zeitschrift der Deutschen Gesellschaft für Geowissenschaften* **157**, 585–95.

QUESADA, C., FONSECA, P., MUNHÁ, J., OLIVEIRA, J. & RIBEIRO, A. 1994. The Beja-Acebuches Ophiolite (Southern Iberia Variscan Foldbelt): geological characterization and geodynamic significance. *Boletín Geológico y Minero de España* **105**(1), 3–49.

RIBEIRO, A., ANTUNES, M. T., FERREIRA, M. P., ROCHA, R. B., SOARES, A. F., ZBYSZEWSKI, G., ALMEIDA, F. M., CARVALHO, D. & MONTEIRO, J. H. 1979. *Introduction à la Géologie Générale du Portugal*. Lisboa: Serviços Geológicos de Portugal, pp. 114.

RIBEIRO, M. A., CRUZ, C. & MARTINS, H. 2013. Metamorfismo do encaixante de Santa Eulália. In *Plutões Graníticos: da Génese à Instalação. Técnicas e Metodologias de Estudo.* Workshop, livro de resumos 4. November 2013, Porto.

RIBEIRO, A., MUNHÁ, J., DIAS, R., MATEUS, A., PEREIRA, E., RIBEIRO, L., FONSECA, P., ARAÚJO, A., OLIVEIRA, T., ROMÃO, J., CHAMINÉ, H., COKE, C. & PEDROS, J. 2007. Geodynamic evolution of the SW Europe Variscides. *Tectonics* **26**, TC6009, doi: 10.1029/2006TC002058.

RIBEIRO, A., MUNHÁ, J., FONSECA, P., ARAÚJO, A., PEDRO, J., MATEUS, A., TASSINARI, C., MACHADO, G. & JESUS, A. 2010. Variscan ophiolite belts in the Ossa-Morena Zone (Southwest Iberia): geological characterization and geodynamic significance. *Gondwana Research* **17**, 408–21.

ROEDDER, E. 1984. Fluid inclusions. In *Reviews in Mineralogy*, vol. 12 (ed. P. E. Ribbe), pp. 644. Mineralogical Society of America.

SANCHEZ-CARRETERO, R., EGUILUZ, L., PASCUAL, E. & CARRACEDO, M. 1990. Igneous rocks. In *Pre-Mesozoic Geology of Iberia* (eds R. D. Dallmeyer & E. Martínez García), pp. 292–313. Berlin: Springer-Verlag.

SANDGREN, P. & THOMPSON, R. 1990. Mineral magnetic characteristics of podzolic soils developed on sand dunes in the Lake Gosciaz catchment, central Poland. *Physics of the Earth and Planetary Interiors* **60**, 297–313.

SANT'OVAIA, H., BOUCHEZ, J. L., NORONHA, F., LEBLANC, D. & VIGNERESSE, J. L. 2000. Composite-laccolith emplacement of the post-tectonic Vila Pouca de Aguiar granite pluton (northern Portugal): a combined AMS and gravity study. *Transactions of the Royal Society of Edinburgh: Earth Sciences* **9**, 123–37.

SANT'OVAIA, H., OLIVIER, P., FERREIRA, N., NORONHA, F. & LEBLANC, D. 2010. Magmatic structures and kinematics emplacement of the Hercynian granites from Central Portugal (Serra da Estrela and Castro Daire areas). *Journal of Structural Geology* **32**, 1450–65.

SCHERMERHORN, L. J. G., PRIEM, H. N. A., BOELRIJK, N. A. I. M., HEBEDA, E. H., VERDURMEN, E. A. TH. & VERSCHURE, R. H. 1978. Age and origin of the Messejana Dolerite Fault-Dike System (Portugal and Spain) in the light of the opening of the North Atlantic Ocean. *The Journal of Geology* **86**(3), 229–309.

SHEPHERD, T. J., RANKIN, A. H. & ALDERTON, D. H. M. 1985. *A Pratical Guide to Fluid Inclusion Studies*. Glasgow: Blackie & Son Ltd.

SIMANCAS, J. F., CARBONELL, R., GONZÁLEZ LODEIRO, F., PÉREZ ESTAÚN, A., JUHLIN, C., AYARZA, P., KASHUBIN, A., AZOR, A., MARTÍNEZ POYATOS, D., ALMODÓVAR, G. R., PASCUAL, E., SÁEZ, R. & EXPÓSITO, I. 2003. The crustal structure of the transpressional Variscan Orogen of SW Iberia (IBERSEIS). *Tectonics* **22**(6), 1962–74.

SIMANCAS, J. F., MARTÍNEZ POYATOS, D. J., EXPÓSITO, I., AZOR, A. & GONZÁLEZ LODEIRO, F. 2001. The structure of a major suture zone in the SW Iberian Massif: the Ossa Morena/Central Iberian contact. *Tectonophysics* **332**, 295–308.

SMITH, D. L. & EVANS, B. 1984. Diffusional crack healing in quartz. *Journal of Geophysical Research* **89**, 4125–35.

SYLVESTER, A. 1998. Magma mixing, structure, and re-evaluation of the emplacement mechanism of Vrådal pluton, central Telemark, southern Norway. *Norsk Geologisk Tidsskrift* **78**, 259–76.

TARLING, D. H. & HROUDA, F. 1993. *The Magnetic Anisotropy of Rocks*. London: Chapman and Hall, 217 pp.

THOMPSON, R. & OLDFIELD, F. 1986. *Environmental Magnetism*. London: Allen & Unwin, 227 pp.

ŽÁK, J., HOLUB, F. V. & KACHLÍK, V. 2006. Magmatic stoping as an important emplacement mechanism of Variscan plutons: evidence from roof pendants in the Central Bohemian Plutonic Complex (Bohemian Massif). *International Journal of Earth Sciences* **95**(5), 771–89.